

# Effects of Sodium and Tungsten Promoters on Mg<sub>6</sub>MnO<sub>8</sub> Based Core-Shell Redox Catalysts for Chemical Looping – Oxidative Dehydrogenation of Ethane

Seif Yusuf<sup>1</sup>, Luke Neal<sup>1</sup>, Zhenghong Bao<sup>2</sup>, Zili Wu<sup>2</sup>, and Fanxing Li<sup>1\*</sup>

<sup>1</sup> Department of Chemical and Biomolecular Engineering, North Carolina State University, 911 Partners Way, Raleigh, North Carolina, 27695-7905, United States.

<sup>2</sup> Center for Nanophase Materials Sciences and Chemical Science Division, Oak Ridge National Laboratory, Oak Ridge, Tennessee 37831, United States

\* Corresponding author. Email: [fli5@ncsu.edu](mailto:fli5@ncsu.edu)

## **Abstract**

The present study investigates the effect of sodium and tungsten promoters on Mg<sub>6</sub>MnO<sub>8</sub> based redox catalysts in a chemical looping oxidative dehydrogenation (CL-ODH) scheme. CL-ODH has the potential to significantly lower energy consumption and CO<sub>2</sub>/NO<sub>x</sub> emissions for ethylene production compared to conventional steam cracking. Sodium tungstate (Na<sub>2</sub>WO<sub>4</sub>) was shown to be an effective promoter for Mg<sub>6</sub>MnO<sub>8</sub> based redox catalysts. Overall, the CL-ODH reaction proceeds via parallel gas phase cracking of ethane and selective combustion of H<sub>2</sub> on the surface of the Na<sub>2</sub>WO<sub>4</sub> promoted redox catalyst. Reaction testing indicated that both Na and W are necessary to form Na<sub>2</sub>WO<sub>4</sub> and to achieve high ethylene selectivity. A Na:W ratio lower than 2:1 lead to significant formation of additional mixed tungsten oxide phases and decreases ethylene selectivity. Further characterizations based on Low Energy Ion Scattering (LEIS) and differential scanning calorimetry (DSC) indicate that the NaW promoter forms a molten shell around the Mg<sub>6</sub>MnO<sub>8</sub> redox catalyst. Methanol TPSR and *in-situ* DRIFTS experiments indicate that the promoter significantly suppresses the number of basic sites on Mg<sub>6</sub>MnO<sub>8</sub>. <sup>18</sup>O-<sup>16</sup>O exchange experiments reveal that the promoter decreases the rate of oxygen exchange. O<sub>2</sub> co-feed studies indicate that below the melting temperature of Na<sub>2</sub>WO<sub>4</sub>, H<sub>2</sub> and CO conversions are both inhibited,

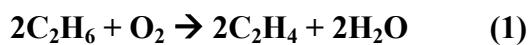
but above the melting temperature H<sub>2</sub> combustion significantly increased while CO combustion is still inhibited. Based on extensive characterizations, it was determined that H<sub>2</sub> is primarily combusted at the gas-Na<sub>2</sub>WO<sub>4</sub> molten shell interface via redox reactions of the tungsten salt, likely between the WO<sub>4</sub><sup>2-</sup> (tungstate) and WO<sub>3</sub><sup>-</sup> (tungsten bronze).

**Keywords:** *oxidative dehydrogenation, chemical looping, redox catalyst, oxygen carrier*

## **Introduction**

Ethylene is a valuable commodity chemical and an important building block for numerous compounds including oxygenates, polymers and various chemical intermediates<sup>1</sup>. Due to the significant fraction of ethane in shale gas (up to 20 vol%)<sup>2,3</sup>, it has become an abundant and economically attractive feedstock for ethylene production. Currently, ethane and other hydrocarbon feedstocks, e.g. naphtha and gas oil, are used to produce ethylene through steam cracking, a commercial process where ethane undergoes high temperature pyrolysis in the presence of diluting steam<sup>4</sup>. In steam cracking of ethane, a mixture of ethane and steam is preheated and then fed into high temperature reactor tubes for gas phase cracking reactions<sup>5</sup>. There are multiple challenges and drawbacks that this process faces: 1) the single pass conversion is equilibrium limited, 2) the formation of coke requires periodic shutdown of reactors<sup>6</sup>, 3) there are significant amounts of both CO<sub>2</sub> and NO<sub>x</sub> emissions and 4) there is a high energy demand for this process (16GJ/ton of ethylene produced) due to the highly endothermic cracking reactions and complex downstream separations<sup>1,4</sup>.

An alternative to steam cracking is the oxidative dehydrogenation (ODH) of ethane<sup>5,7-10</sup>. In this reaction (reaction 1), oxygen is used to combust hydrogen, removing equilibrium constraints on ethane conversion and makes the overall reaction exothermic.



Despite of its various potential advantages, ethane ODH faces a number of practical challenges including (i) the co-feeding of oxygen and ethane imposes potential safety hazards and hence significant inert gas dilution is required and (ii) oxygen generation via air separation can be both capital and energy intensive<sup>11</sup>. In addition, limited ethylene selectivity is often reported at high single-pass ethane conversions.

In order to address these challenges, we have previously proposed chemical looping-oxidative dehydrogenation (CL-ODH) (Figure 1)<sup>11-16</sup>. CL-ODH is similar other chemical looping redox systems that have been used to various applications including oxygen uncoupling(CLOU)<sup>17-19</sup>, and the partial oxidation of methane<sup>20-24</sup>. In CL-ODH, a redox catalyst, also known as oxygen carrier, donates oxygen from its lattice to convert ethane to ethylene and water in an ODH reactor. After the redox catalyst is reduced, it is transferred to an air reactor where it is re-oxidized in air and then transferred back to the ODH reactor to complete the redox cycle. This process removes the drawbacks from the ODH reaction as it does not require an air separation unit and eliminates the safety concerns from the co-feeding of oxygen and ethane. Additionally, process simulations have indicated that the CL-ODH process can reduce energy consumption and CO<sub>2</sub> emissions by up to 82% when compared to steam cracking<sup>11</sup>.

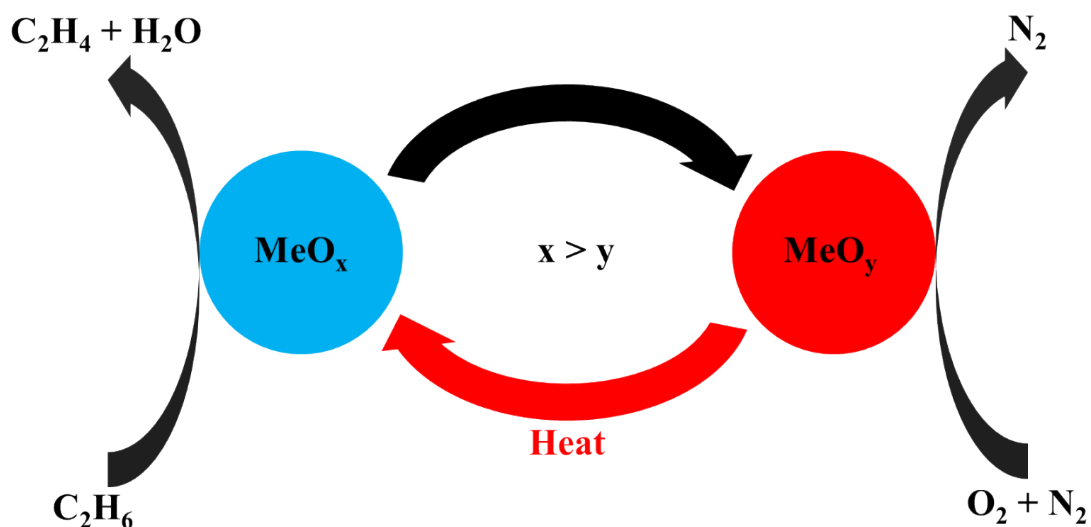


**Figure 1:** Simplified schematic of the CL-ODH process. ODH step is shown on the left and re-oxidation step is shown on the right.

Vanadium-oxide-based redox catalysts have previously been studied for the CL-ODH of ethane<sup>25,26</sup>, but the ethylene yields were typically below 15% due to the low conversion of ethane (between 7 and 25%) and a drop in ethylene selectivity at higher ethane conversions (from 85% to 58%). Iron based perovskites were able to achieve significantly higher ethylene yields (up to 55%) but had low oxygen capacities (<0.7wt%) at 700°C<sup>15,16</sup>. The highest ethylene and light olefin selectivity (~92% total) with an ethane conversion of 76.2% were obtained from  $\text{Na}_2\text{WO}_4$  promoted  $\text{Mg}_6\text{MnO}_8$  redox catalysts in our previous study<sup>12</sup>. Reaction testing also indicated that both sodium and tungsten need to be present on the surface of the redox catalyst in order to maximize ethylene yield. However, the exact nature and role of the  $\text{Na}_2\text{WO}_4$  promoter on  $\text{Mg}_6\text{MnO}_8$  based redox catalyst has still not been determined. This study focuses on the optimization of NaW based promoters on  $\text{Mg}_6\text{MnO}_8$  redox catalysts and gaining further insight into the nature of the NaW promoter through comprehensive characterization of the redox catalysts.

## **Experimental**

### **Redox Catalyst Synthesis**

All the redox catalysts (un-promoted and NaW promoted) were synthesized through an incipient wetness impregnation method described in our previous study<sup>12</sup>. Manganese (II) nitrate (Sigma-Aldrich, 98%) and magnesium oxide powder (Materion Advanced Chemicals,  $\geq 99.5\%$ ) were used in all redox catalysts. For the NaW promoted redox catalysts, the promoter precursors were sodium tungstate dihydrate (Sigma-Aldrich,  $\geq 99\%$ ), sodium nitrate (Fisher,  $\geq 99\%$ ) and ammonium meta tungstate (Sigma-Aldrich,  $\geq 85\%$  WO<sub>3</sub> basis). Sodium tungstate dihydrate was used for the 2:1 redox catalyst and a combination of sodium nitrate and ammonium meta tungstate was used for all other Na:W molar ratios of 4:1, 1:1 and 1:2. For all of the previously listed Na:W ratios, the final sodium loading was 1.7 wt%. This loading is within the range of alkali doping on previously reported systems<sup>27,28</sup>. An additional Na:W = 1:1 redox catalyst where the tungsten loading was kept the same, but the sodium loading was halved to 0.85wt% was also synthesized and is referred to as Na:W = 1:1 (0.5Na).

### **Ethane ODH experiments**

Reaction testing was performed using the same quartz U-tube reactor setup as described in our previous study<sup>12</sup>. In order to determine the activity of the catalysts, redox cycle experiments were performed. During the reduction step, 80% C<sub>2</sub>H<sub>6</sub> balance Ar was used, and during the re-oxidation step the gas was switched to 17% O<sub>2</sub> balance Ar. After each reduction and oxidation step, 100% Ar was flowed to purge the reactor. The reactor gas manifold is configured such that the total flow rate into the reactor does not change between the purge and reduction steps. Before ODH testing, the redox catalysts were pretreated with 3 redox cycles comprising of a 3 minute reduction step and 3 minute oxidation step at 900 °C to obtain a redox catalyst with stabilized

chemical and physical properties. During ODH redox cycles, a GHSV of 4500 hr<sup>-1</sup> and temperature of 850 °C was used for initial testing of the redox catalysts. During the reduction step, 5 mL of ethane was flowed into the reactor and the re-oxidation step was 3 minutes. The purge step between the reduction and oxidation steps was 5 minutes.

The products from the reduction and oxidation steps were collected in a gas sampling bag and characterized using a gas chromatograph (GC). An Agilent 7890 Series Fast RGA GC with two thermal conductivity detector (TCD) channels (He/TCD channel for CO/CO<sub>2</sub> analysis, Ar/TCD channel for H<sub>2</sub> analysis), and a flame ionization detector (FID) channel for hydrocarbon analysis was used. The system was calibrated using a refinery gas calibration standard (Agilent Part # 5190-0519). The selectivity and conversion values for carbonaceous species were calculated relative to the carbon mass balance. The total amounts of hydrogen formed and converted to water were calculated by hydrogen mass balance of all recovered species.

### **Redox Catalyst Characterizations**

Phase identification of as-prepared redox catalysts was performed using Powder X-Ray Diffraction (XRD). A Rigaku SmartLab X-ray Diffractometer with Cu K $\alpha$  ( $\lambda = 0.1542$  nm) radiation operating at 40 kV and 44 mA. A scanning range of 10-80° (2 $\theta$ ) with a step size of 0.1° holding for 3.5 seconds at each step was used to generate XRD patterns.

Low Energy Ion Scattering (LEIS) analysis was performed at the Surface Analysis Center at Lehigh on an ION\_TOF Qtaz<sup>100</sup> spectrometer to obtain surface compositional information. A 3 keV He<sup>+</sup> (2 X 10<sup>14</sup> ions cm<sup>-2</sup>, 1.0 X 1.0 mm raster) primary ion beam was used at 3000 eV pass energy, while a 0.5 keV sputtering source (0.5 or 1.0 X 10<sup>15</sup> cm<sup>-2</sup> cyc<sup>-1</sup>, 2.0 X 2.0 mm or 1.5 X 1.5 mm raster was used at 30° angle to the sample surface for depth profiling); during spectra

acquisition and sputtering, charge neutralization was invoked. Prior to analysis, sample powders were dispersed into a sample holder and compressed by 2000 psi.

Methanol Temperature Programmed Surface Reaction (TPSR) experiments were performed to analyze the nature of the active sites of  $\text{Mg}_6\text{MnO}_8$  based redox catalysts. Un-promoted and NaW promoted (Na:W = 2:1 and 1:2) redox catalysts were tested. 1 g of redox catalyst was loaded into a quartz u-tube reactor and was cleaned in 10%  $\text{O}_2$  balance He at  $850^\circ\text{C}$  for 30 minutes and then cooled down to room temperature. The gas flow was switched to 100% He and flown through a vessel with methanol at room temperature for 1 hour. The flow was then switched to bypass the methanol vessel and the reactor was heated up to  $110^\circ\text{C}$  and held there for 2 hours to remove physically adsorbed methanol. Next, the temperature was then ramped at  $10^\circ\text{C}$  per minute to  $600^\circ\text{C}$  and held at that temperature for 10 minutes. All products were analyzed using a Quadrupole Mass Spectrometer (QMS, MKS Cirrus II) and then a heated line was used to ensure that products stayed in the gas phase before being analyzed.

*In-Situ* Diffuse Reflectance Infrared Fourier Transform Spectroscopy (DRIFTS) study was performed with methanol as a probe molecule to study the surface of  $\text{Mg}_6\text{MnO}_8$  based redox catalysts. A Thermo Fisher Nicolet iS50 FT-IR with a Pike Technologies DiffusIR sample chamber/unit was used to take in-situ spectra of the redox catalyst at different temperatures and conditions. The two redox catalysts studied were the un-promoted and Na:W= 2:1. After being loaded into the porous alumina crucible, the redox catalyst was heated to  $750^\circ\text{C}$  in 10%  $\text{O}_2$  balance Ar. The catalyst was then cooled down in  $50^\circ\text{C}$  increments and background spectra were taken at each step. At  $50^\circ\text{C}$ , the flow was switched to 100% Ar and flown through a vessel with methanol at room temperature for 2 hours. The sample chamber was then purged for 1 hour in 100% Ar. Afterwards, a spectrum was taken at  $50^\circ\text{C}$  and then the temperature was raised in  $50^\circ\text{C}$

increments, with a spectrum taken at each increment. Each spectrum taken after methanol adsorption was processed using the background spectrum at the corresponding temperature and the Kubelka-Munk model.

$^{18}\text{O}$ - $^{16}\text{O}$  isotope exchange experiments were performed on un-promoted and Na:W=2:1 redox catalysts as described by Bouwmeester et al.<sup>29,30</sup> 45mg of redox catalyst was loaded into a 1/4" O.D. x 1/8" I.D quartz U-tube reactor and was heated to temperature under a 5%  $^{16}\text{O}_2$  flow balance Ar. Once at temperature, 1mL pulses of 5%  $^{18}\text{O}_2$  was injected into the reactor. A total of 5 pulses 3 minutes apart were injected.  $m/z = 34$  and  $36$  were measured on a QMS, to determine the amount of oxygen exchange in each pulse. Nitrogen ( $m/z = 28$ ) was tracked in order to determine the integration limits for each pulse. A room temperature pulse injection was used to determine a pulse where oxygen exchange did not occur. The initial temperature tested was 650 °C and the temperature was raised in 50 °C increments to 850 °C. The integrated QMS data was used to determine the exchange rate of oxygen and activation energies.

### **CO-O<sub>2</sub>/ H<sub>2</sub>-O<sub>2</sub> co-feed experiments**

The conversion of CO and H<sub>2</sub> in co-feed (with O<sub>2</sub>) conditions over the un-promoted and Na:W=2:1 redox catalysts were measured. The same quartz U-tubes used in Ethane ODH reaction testing, including the blank were used for the co-feed experiments. For CO-O<sub>2</sub> co-feed experiments, each sample was initially cleaned in 10% O<sub>2</sub> balance Ar at 850 °C for 30 minutes. The temperature was then lowered to 600 °C and the flow was switched to 10%CO/10% O<sub>2</sub> balance Ar. This flow was kept until a steady result was seen on the QMS. The flow was then switched back 10% O<sub>2</sub> balance Ar and the temperature was adjusted. The other 2 temperatures tested was 700 and 800°C. A QMS was used to determine the conversion of carbon monoxide. The same

procedure was used for H<sub>2</sub>-O<sub>2</sub> co-feed experiments except the flow during testing was 2% H<sub>2</sub>, 2% O<sub>2</sub> balance argon and the temperatures measured were 600 and 700 °C.

Details of several additional characterizations performed such as *in-situ* Raman experiments and the redox nature of Na<sub>2</sub>WO<sub>4</sub> can be found in the supplementary information.

## Results and Discussion

### Redox Catalyst Characterization

XRD patterns of as-prepared redox catalysts are shown in Figure 2. For all the redox catalysts, the characteristic peaks of the Mg<sub>6</sub>MnO<sub>8</sub> phase (PDF# 01-074-1903) were observed. The Na<sub>2</sub>WO<sub>4</sub> (PDF#04-008-8508) and Na<sub>4</sub>MgW<sub>3</sub>O<sub>12</sub> (PDF# 01-083-6809) phases were also observed in the promoted redox catalysts. The relative intensity of the Na<sub>2</sub>WO<sub>4</sub> characteristic peaks initially increases as the Na:W ratio decreases from 4:1 to 2:1, but then decreases as the Na:W ratio further decreases to 1:2. The strength of the characteristic peaks for Na<sub>4</sub>MgW<sub>3</sub>O<sub>12</sub> stayed the same, until Na:W = 1:2 redox catalyst where the relative intensity increased. The MgWO<sub>4</sub> (PDF# 04-006-9803) phase was also detected on the Na:W=1:2 redox catalyst. On the Na:W= 1:1 (0.5 Na) redox catalyst, all four of the previously mentioned phases were detected. Na<sub>4</sub>MgW<sub>3</sub>O<sub>12</sub> and MgWO<sub>4</sub> phases were more significant on the Na:W= 1:1 (0.5 Na) redox catalyst when compared to the Na:W=1:1 redox catalyst, indicating that a lack of sodium leads to formation of additional tungsten oxide phases.

In order to determine if the NaW promoter has an effect on the crystal structure of the base Mg<sub>6</sub>MnO<sub>8</sub> redox catalyst, Rietveld refinement was performed on the un-promoted and the Na<sub>2</sub>WO<sub>4</sub> promoted Mg<sub>6</sub>MnO<sub>8</sub> redox catalysts. Information about XRD spectra and Rietveld refinement results can be found in the supplementary information file (Figure S1). There were no significant

differences in the lattice parameters between the two redox catalysts, indicating that  $\text{Na}_2\text{WO}_4$  and  $\text{Mg}_6\text{MnO}_8$  are separate crystal phases in the redox catalyst.

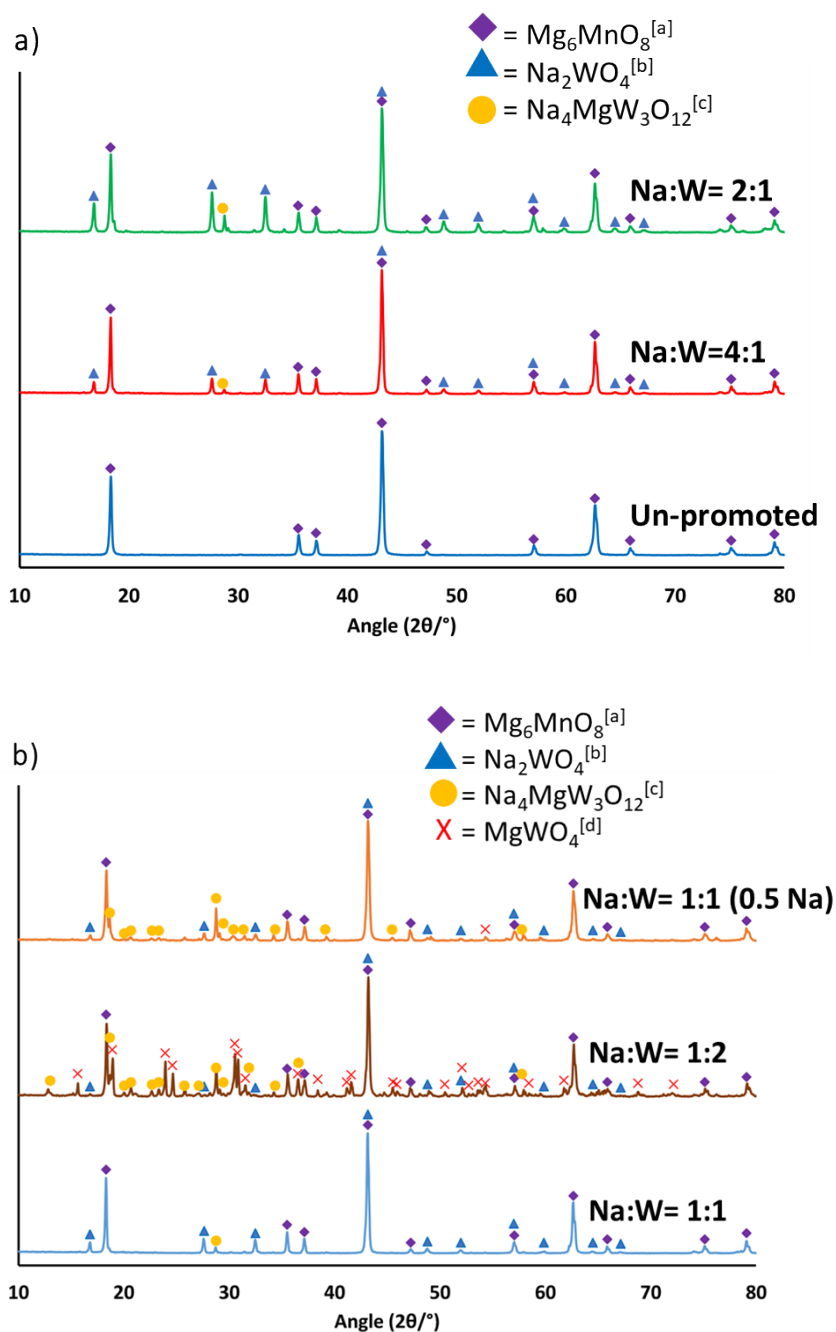


**Figure 2:** XRD patterns of as-prepared redox catalysts (a) un-promoted, Na:W=4:1 and Na:W=2:1 redox catalysts. (b) Na:W=1:1, Na:W=1:2, and Na:W= 1:1 (0.5 Na) redox catalysts. [a]PDF# 01-074-1903 [b]PDF# 04-008-8508 [c]PDF#01-083-6809 [d]PDF# 04-006-8508

## ODH Reaction Testing

Figure 3 summarizes ethane ODH testing at 850 °C and a GHSV of 4500 hr<sup>-1</sup> for all the redox catalysts synthesized. When compared to the blank (thermal cracking), all the redox catalysts show an increase in ethane conversion. Previous studies have determined that a H<sub>2</sub> conversion of 70% is desired for the CL-ODH process from a process energy balance standpoint<sup>11</sup> and all of the promoted catalysts show H<sub>2</sub> conversion well above 70%. While the un-promoted redox catalyst has the highest ethane conversion (94.60%), it has the lowest ethylene yield (13.29%) due to high CO<sub>x</sub> selectivity (83.48%). After the addition of sodium and tungsten at any ratio, there is a significant increase in the ethylene yield. This increase in ethylene yield occurs despite a decrease in ethane conversion, due to the larger increase in ethylene selectivity and decrease in CO<sub>x</sub> selectivity. The two best performing redox catalysts were Na:W = 2:1 and 1:1 with ethylene yields of 62.17% and 62.91%, respectively.

The effect of sodium loading can be determined through testing of the Na:W = 1:1 (0.5Na) redox catalyst. When compared the standard (1.7 wt.% Na) Na:W = 1:1, the ethylene yield decreased slightly from 62.91% to 61.12%. The decrease in ethylene yield, which is primarily resulted from increased CO<sub>x</sub> selectivity, further confirms the importance of Na and W in suppressing CO<sub>x</sub> formation. In terms of the effect of Na and W ratio, our previous study indicates that a lack of W leads to loss of Na from the surface and increased CO<sub>x</sub> selectivity<sup>12</sup>. The current study indicates that lowering the Na:W to less than 1:1 is also not desirable, as can be seen from the lowered ethylene yield for the Na:W = 1:2 sample. This decrease may have resulted from the formation of additional tungsten containing phases other than Na<sub>2</sub>WO<sub>4</sub>.

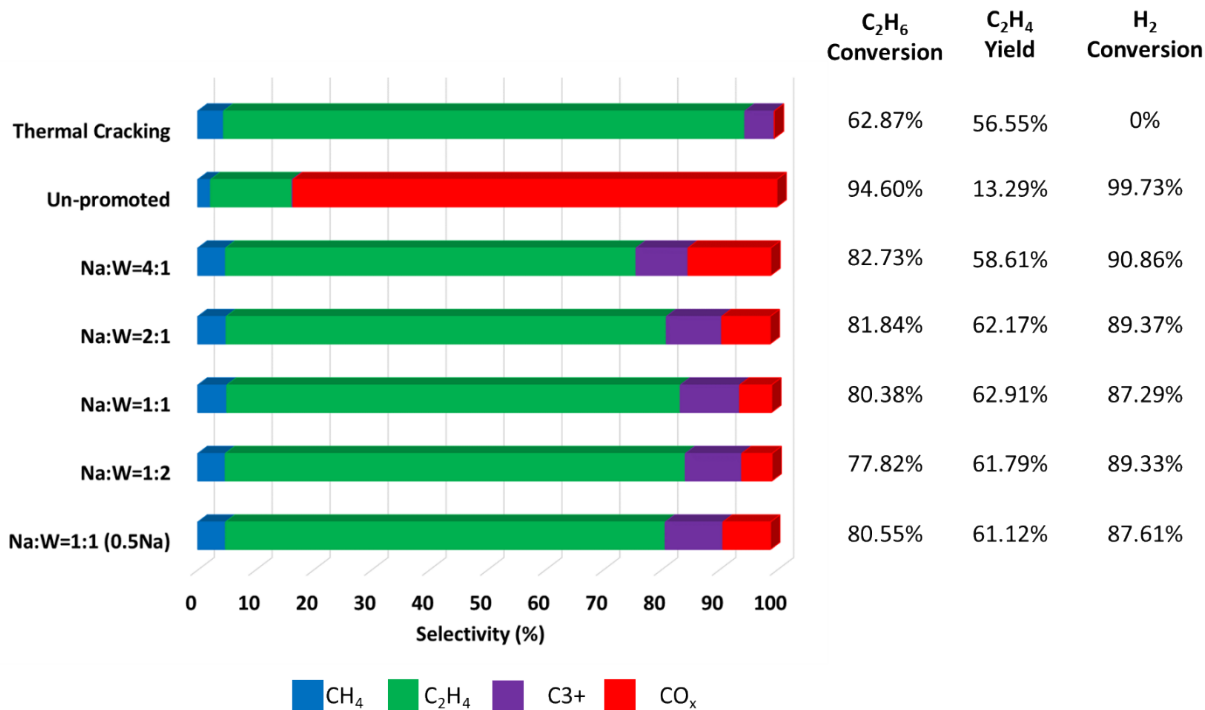


**Figure 3:** ODH reaction data at 850 °C and GHSV=4500 hr<sup>-1</sup> for thermal cracking (blank) and all the redox catalysts

In Figure 4, the effects of reaction temperature on the performance of selected redox catalysts are shown. All of the promoted redox catalysts exhibited comparable ethane conversion and ethylene selectivity (Figure 4a). More noticeable differences can be seen between the CO<sub>x</sub> selectivity values of the promoted redox catalysts (Figure 4b). At 850 °C, the Na:W = 2:1 and Na:W = 1:1 (0.5Na) redox catalysts showed similar CO<sub>x</sub> selectivity (~8.3%) while the Na:W=1:1 redox catalyst exhibited a lower CO<sub>x</sub> selectivity of 5.52%. As the temperature decreases, the difference between the redox catalysts CO<sub>x</sub> selectivity values decrease, but the Na:W = 1:1 (0.5Na) always exhibited the highest CO<sub>2</sub> selectivity. Due to the small differences in activity between the different promoted redox catalysts, further characterization in this study will primarily focus on the un-promoted and Na:W = 2:1 promoted redox catalyst due to its (i) high ethylene yield and (ii)

better defined phase compositions, i.e.  $\text{Na}_2\text{WO}_4$  and  $\text{Mg}_6\text{MnO}_8$  were the predominant phases with negligible amount of  $\text{Na}_4\text{MgW}_3\text{O}_{12}$  phase (Figure 2a).

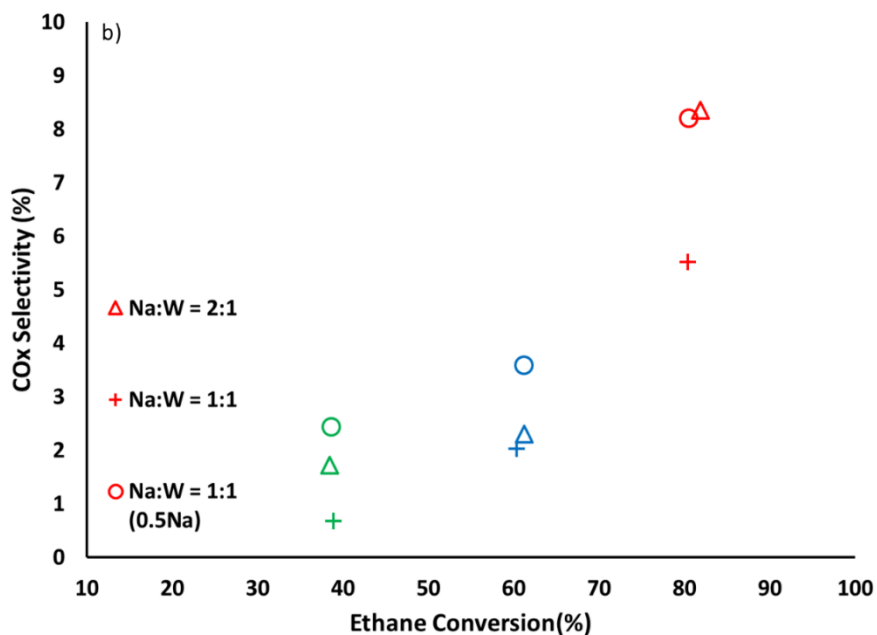
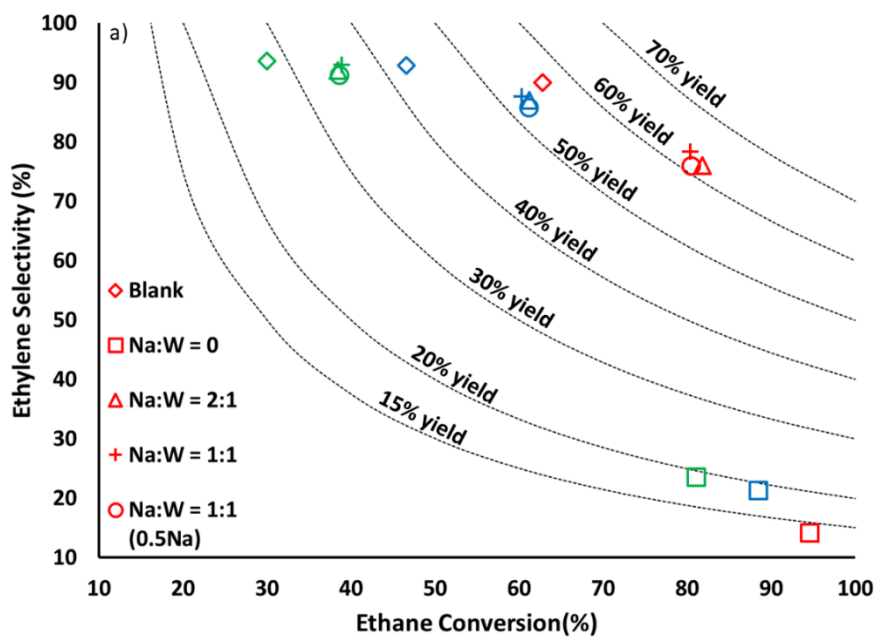


**Figure 4:** ODH reaction data at varying temperatures a) Ethylene Selectivity vs ethane conversion and b) CO<sub>x</sub> selectivity vs ethane conversion (Green: 800 °C, Blue: 825 °C, Red: 850 °C and GHSV=4500 hr<sup>-1</sup>).

## Surface Characterization of the Redox Catalyst

### *LEIS Analysis*

Our previous XPS study on promoted  $\text{Mg}_6\text{MnO}_8$  based redox catalysts showed an enrichment of sodium and tungsten on the surface of the Na:W =2:1 promoted catalyst<sup>12</sup>. The  $\text{Na}_2\text{WO}_4$  promoter also suppressed the amount of Mn atoms on the surface and lowered the average oxidation of Mn. While XPS can analyze the near-surface region of the catalyst, the penetration depth of this technique is greater than the first few atomic layers. As such, the true surface composition of the redox catalyst cannot be accurately determined by XPS. A more surface sensitive technique, LEIS was used to determine the surface elemental composition of the redox catalyst. For each catalyst, multiple sputtering cycles with a 0.5 keV  $\text{Ar}^+$  sputtering was done with  $1 \times 10^{15} \text{ Ar}^+$  ions/cm<sup>2</sup> corresponding to one cycle and the removal of approximately one atomic layer. Figure 5 shows the spectra and integrated peak areas for the un-promoted and Na:W = 2:1 promoted redox catalysts. On the un-promoted catalyst, Mg and Mn are the primary elements detected after the first sputtering cycle. Additional sputtering shows increased amounts of Mg, but Mn remain relatively the same. A Ca impurity from the MgO powder used during synthesis was also observed. On the Na:W = 2:1 promoted catalyst, after one sputtering cycle, the primary elements detected were sodium/magnesium (it is difficult to separate these 2 elements due to their similar atomic masses) and tungsten. Even after 10 sputtering cycles, there is significantly less manganese detected than sodium and tungsten. These results indicate that the outermost layers of the redox catalyst are likely to be composed of W and Na (as opposed to Mn). Since the activity of a catalyst is primarily determined by the first few atomic layers<sup>31</sup>, it has been shown that the  $\text{Na}_2\text{WO}_4$  is of significant importance for suppressed  $\text{CO}_x$  formation and increased ethylene yields.

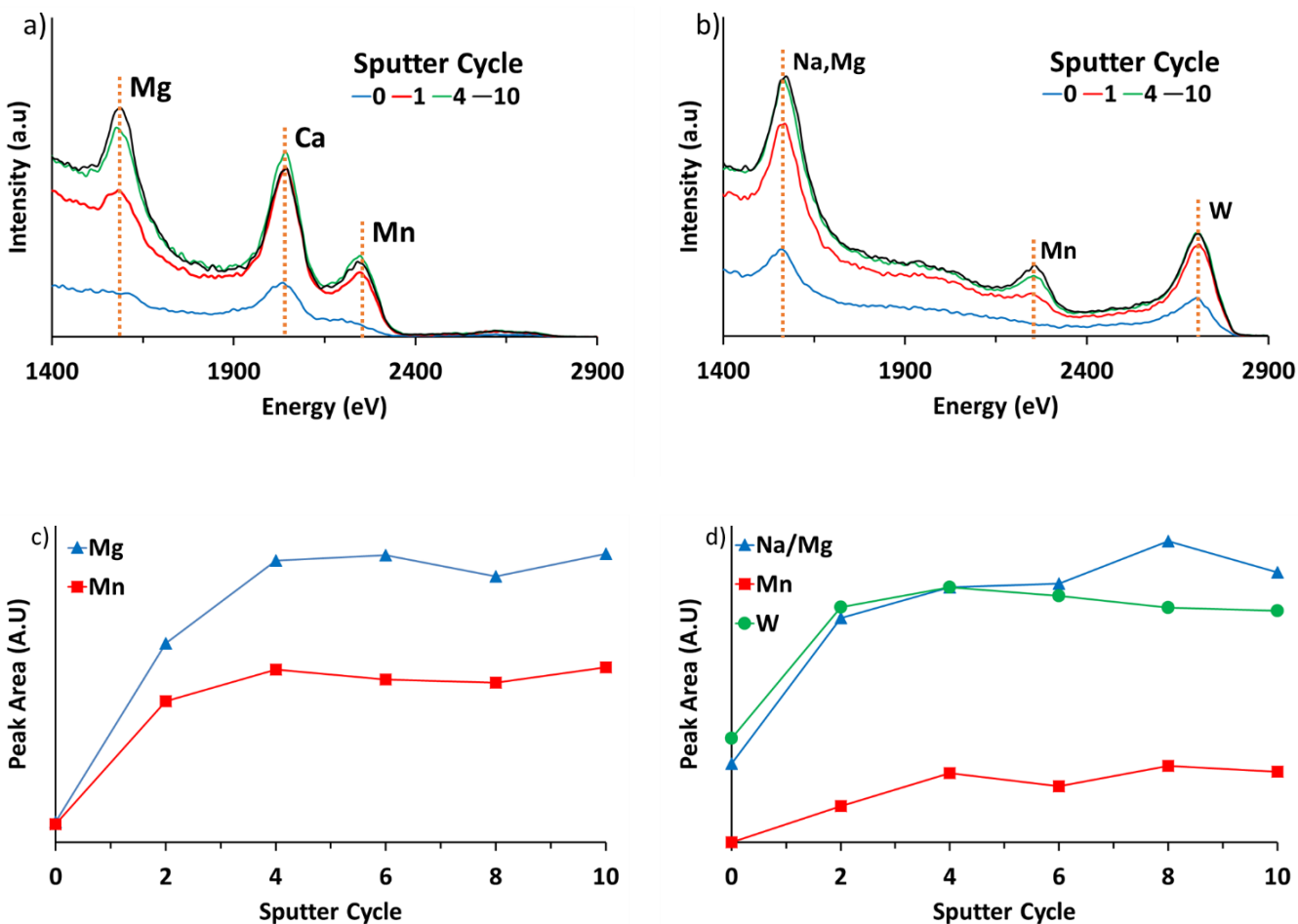


**Figure 5:** LEIS spectra and peak area over sputter cycles for a, c) un-promoted and b, d) Na:W = 2:1 redox catalysts.

### CO-O<sub>2</sub> co-feed study

Data presented in the previous section indicates that the outermost atomic layer of the redox catalyst is covered by Na<sub>2</sub>WO<sub>4</sub>. Differential Scanning Calorimetry (DSC) measurements of the promoted redox catalyst revealed that the Na<sub>2</sub>WO<sub>4</sub> promoter melted at 684 °C, which was close to the melting point (698 °C) of bulk Na<sub>2</sub>WO<sub>4</sub> (Figure S2). This is also consistent with Rietveld Refinement results, which indicated that Na<sub>2</sub>WO<sub>4</sub> and Mg<sub>6</sub>MnO<sub>8</sub> bulk phases were co-existing without solid-state reactions. It is therefore quite possible that the surface of the Mg<sub>6</sub>MnO<sub>8</sub> redox

catalyst is covered by a surface layer of  $\text{Na}_2\text{WO}_4$ . To further quantify the coverage of  $\text{Na}_2\text{WO}_4$  promoter on the surface of  $\text{Mg}_6\text{MnO}_8$ , a series of CO combustion experiment were performed on both unpromoted and  $\text{Na}_2\text{WO}_4$  promoted redox catalysts while co-feeding gaseous  $\text{O}_2$ . The experiments were carried out at below, near, and above the melting point of  $\text{Na}_2\text{WO}_4$ , i.e. 600, 700 and 800 °C. Figure 6 summarizes the CO combustion results for both un-promoted and NaW promoted redox catalysts as well as the thermal blank.

The un-promoted redox catalyst was highly active for catalytic combustion of CO, showing complete conversion of CO at all measured temperatures and significantly higher than the thermal blank. In comparison, the Na:W = 2:1 redox catalyst showed CO conversions comparable to or lower than the thermal blank at all temperatures. These results indicate that: (i)  $\text{Na}_2\text{WO}_4$  inhibits CO combustion activity of  $\text{Mg}_6\text{MnO}_8$  both in its solids and melted forms; (ii) consistent with LEIS results,  $\text{Na}_2\text{WO}_4$  forms a shell to completely cover the surface of  $\text{Mg}_6\text{MnO}_8$  since the promoted redox catalyst showed no increase in CO combustion activity compared to thermal blank.

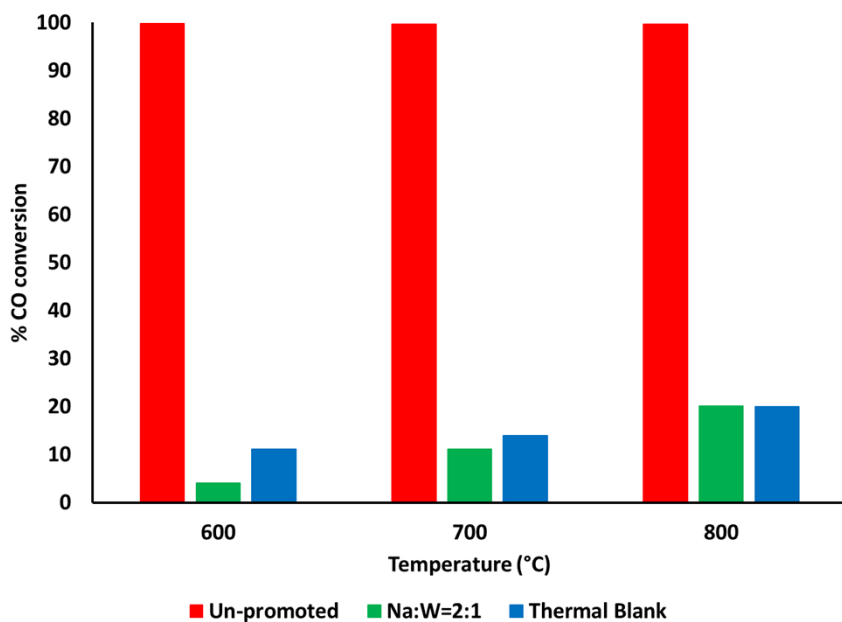


**Figure 6:** Summary of CO- $\text{O}_2$  co-feed study. The gas composition was CO/ $\text{O}_2$ /Ar in a 10/10/80 ratio (vol%).

## **Effect of the Sodium Tungstate Shell**

In order to further investigate the effect of the  $\text{Na}_2\text{WO}_4$  promoter shell on the redox catalyst, various surface characterizations and exchange studies were performed to determine the acid/base/redox properties, activity, and oxygen exchange behavior of the surface.

Methanol TPSR experiments were performed to determine the change in the nature of the active sites on the surface of the redox catalyst after promotion. Previous studies have shown that products that desorb off the catalyst during the temperature ramp after methanol adsorption can be used to determine whether the active sites are basic, acidic, or redox in nature<sup>32</sup>. The three potential products during TPSR runs were carbon dioxide ( $m/z = 44$ ), dimethyl ether ( $m/z = 46$ ), and formaldehyde ( $m/z = 29$ ) for basic, acidic and redox sites respectively. For these studies, the un-promoted, Na:W = 2:1 and Na:W = 1:2 promoted catalyst were tested.

Over all three tested catalysts, only two products were detected, i.e. carbon dioxide and formaldehyde. These products are expected as both magnesium and manganese are reported to have both basic and redox nature. While tungsten can be acidic, the mixed tungsten oxides that are present on these catalysts do not produce any measurable dimethyl ether even on the sample with W overexpressed (Na:W = 1:2). In Figure 7, a comparison of carbon dioxide and formaldehyde production from chemisorbed methanol over all three redox catalysts are presented. The un-promoted redox catalyst shows the highest production of carbon dioxide followed by the Na:W = 2:1 catalyst and then the Na:W = 1:2 redox catalyst which did not produce any significant amounts of carbon dioxide. On the Na:W = 2:1 redox catalyst, three separate peaks are observed for carbon dioxide at ~384, 483, 600 °C. These peaks can also be seen on the un-promoted catalyst, but they are all greater in magnitude than on the Na:W = 2:1 redox catalyst. On the un-promoted redox catalyst, a small amount of formaldehyde is detected with a peak at 258 °C. The Na:W = 2:1 and

Na:W = 1:2 redox catalysts also produce formaldehyde with slightly decreased peak sizes. Overall, methanol TPSR results indicate that the NaW promoter significantly decreases the number of basic sites on the  $\text{Mg}_6\text{MnO}_8$  surface by decreasing the amount of surface Mg and Mn cations on the redox catalyst as seen on previous XPS and LEIS measurements. It is also interesting to point out that redox sites are still observed on the NaW promoted redox catalysts with less significant inhibition, as shown in Figure 7b.

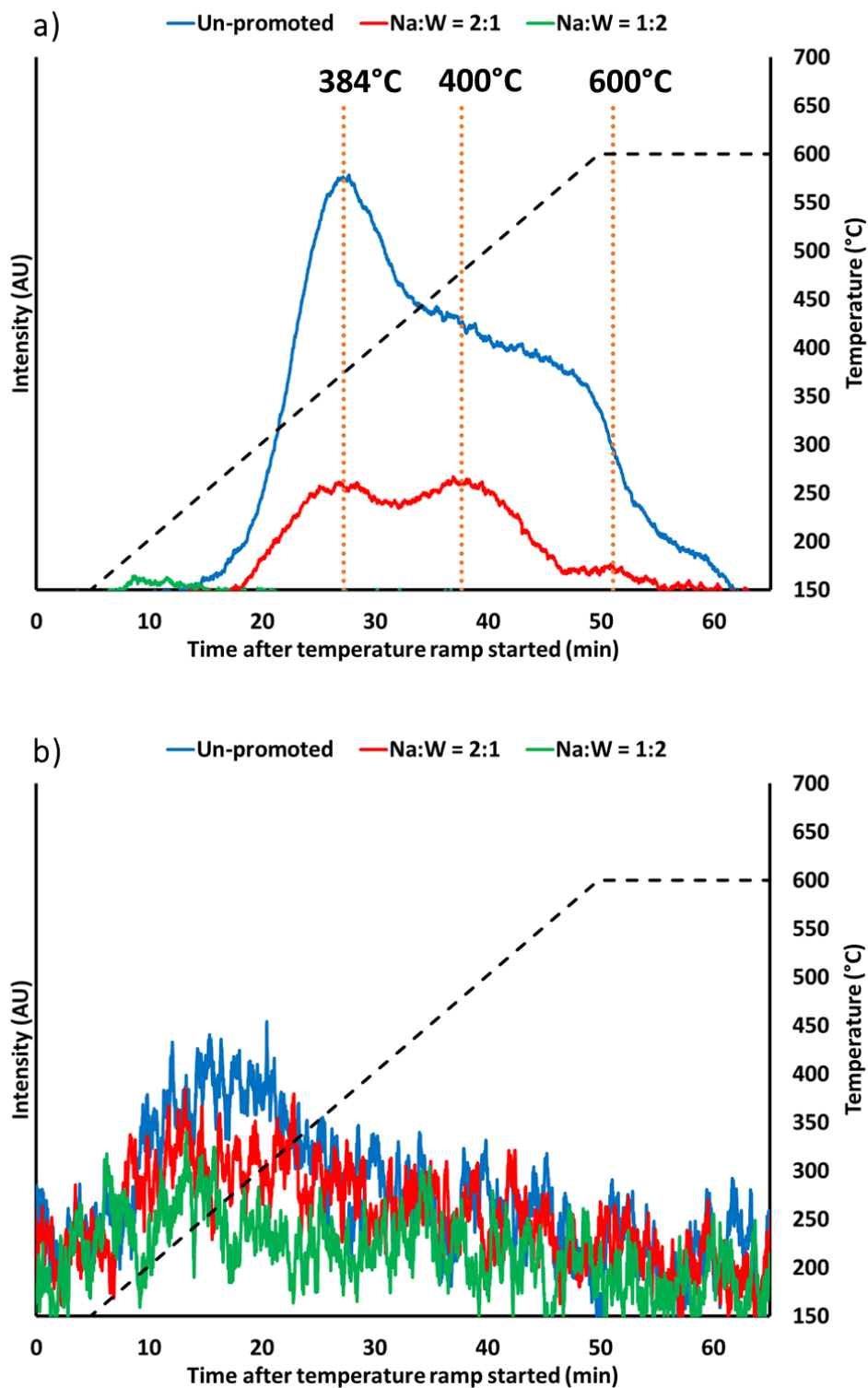


**Figure 7:** Production of a) carbon dioxide and b) formaldehyde from chemisorbed methanol during temperature ramp of methanol TPSR experiments.

*In-situ* DRIFTS experiments were conducted in order to determine surface species formed after methanol adsorption over the un-promoted and Na:W=2:1 promoted redox catalysts. The spectra are resulted from background subtraction (a fully oxidized catalyst surface) at the respective temperature and the Kubelka-Munk model was used so the observed peaks are proportional to their concentrations. Peaks at 1413, 1483, 1594, 2840, 2920, and 2950  $\text{cm}^{-1}$  were observed on the DRIFTS spectra from the redox catalysts. Peaks at 1413 and 1483  $\text{cm}^{-1}$  are associated with carbonate species<sup>33,34</sup> and the peak at 1594  $\text{cm}^{-1}$  is associated with the formate ion that can be found in formic acid and formaldehyde<sup>35-39</sup>, both of which are possible products of methanol oxidation. The peaks at 2840 and 2950  $\text{cm}^{-1}$  are associated with molecularly adsorbed methanol while the peak at 2920  $\text{cm}^{-1}$  is associated with surface methoxy species<sup>40</sup>. Normalized DRIFTS spectra for both redox catalysts can be seen in Figure 8. On the un-promoted redox catalyst, molecularly adsorbed methanol, methoxy and carbonate species are observed at 50 °C. As the temperature increases, the peaks associated with methanol and methoxy decrease in intensity (they are no longer significant at 250 °C and above) while the formate peak appears and grows. The formate peak is at its highest intensity at 250 °C, which is consistent with the peak temperature for formaldehyde observed during methanol TPSR experiments. While carbonate peaks disappeared at 250 °C, they are re-emerged at 350 and 450 °C, indicating conversion of formates to carbonates. The presence of carbonate peaks at these temperatures matches with methanol TPSR data which shows significant  $\text{CO}_2$  production within this temperature range. On the Na:W = 2:1 promoted redox catalyst, only carbonate, molecularly adsorbed methanol and methoxy peaks were observed at 50 °C. The peaks associated with methanol and methoxy are stronger and peaks associated with carbonates are weaker when compared to the un-promoted redox catalyst. When the temperature is increased to 150 °C, peaks associated with methanol and

methoxy decreased significantly and the carbonate peaks grew in intensity. Unlike the un-promoted catalyst, the carbonate peaks were very weak at 250 °C, and no longer present at higher temperatures. Also, no peak associated with formic acid and formaldehyde was observed at any temperatures. These DRIFTS results match with the methanol TPSR results, i.e. the number of basic and redox sites on the surface of un-promoted redox catalyst were largely decreased after promotion with sodium tungstate. As such, *in-situ* DRIFTS study further reinforces that the NaW surface layer inhibits interaction between reactant molecules and the surface of  $\text{Mg}_6\text{MnO}_8$  while exhibiting negligible acid/base or redox properties.

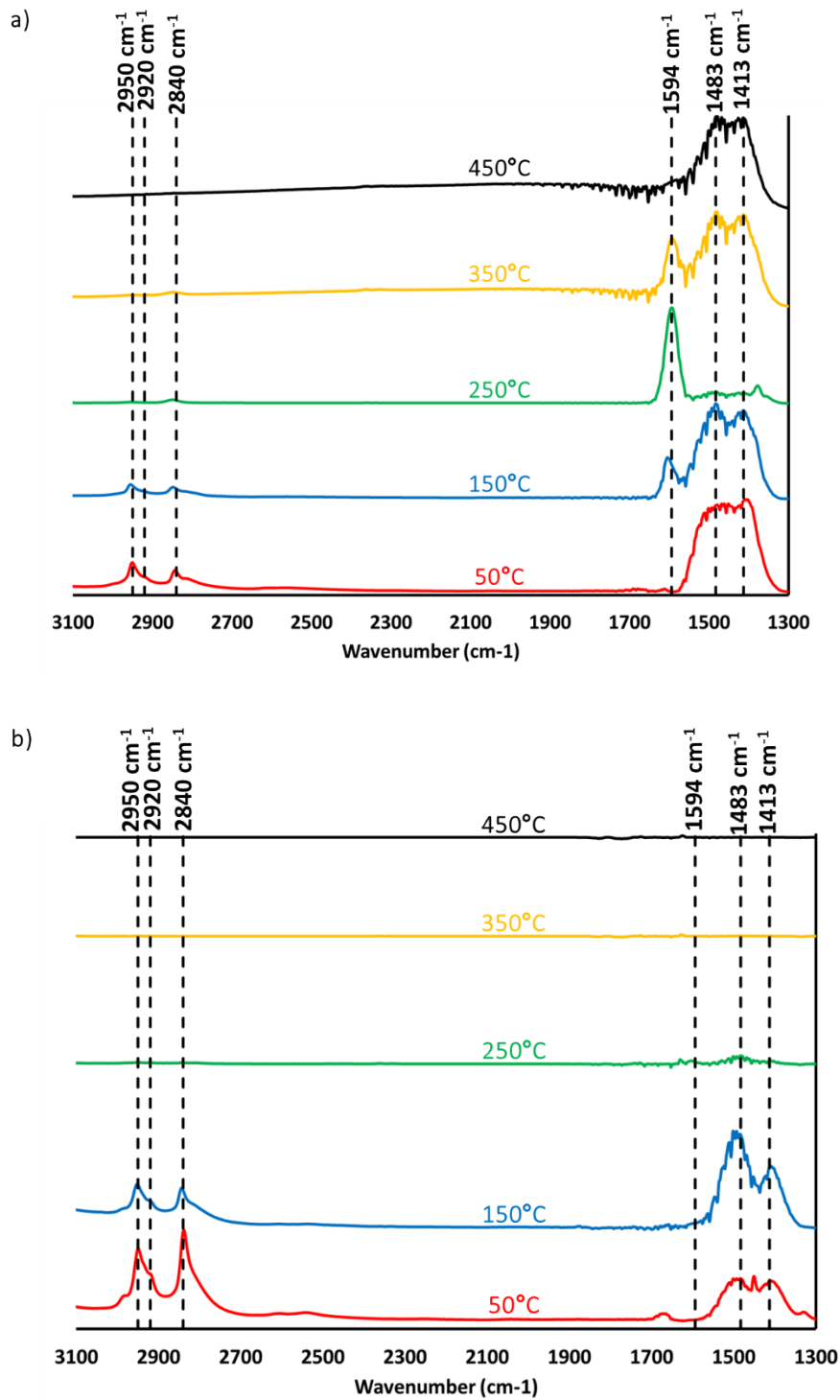
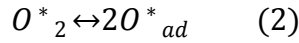


**Figure 8:** *In-Situ* DRIFTS spectra after methanol exposure at 50°C on the a) un-promoted redox catalyst and b) Na:W=2:1 promoted redox catalyst. Adsorbed Methanol: 2950  $\text{cm}^{-1}$  + 2840  $\text{cm}^{-1}$ , Methoxy: 2920  $\text{cm}^{-1}$ , Formate: 1594  $\text{cm}^{-1}$ , Carbonate: 1483  $\text{cm}^{-1}$  + 1413  $\text{cm}^{-1}$

Since the CL-ODH process relies on cyclic donation and re-incorporation of oxygen, rates of oxygen adsorption and incorporation can play an important role towards: i. further understanding of the effect of the Na<sub>2</sub>WO<sub>4</sub> surface layer and ii. the redox activity of the catalyst. <sup>18</sup>O<sub>2</sub>-<sup>16</sup>O<sub>2</sub> exchange experiments were performed to determine the oxygen surface exchange rates of the redox catalysts using the method previously reported by Bouwmeester et al.<sup>29,30</sup> The pulse isotope fractions for the three oxygen species (<sup>16</sup>O<sub>2</sub>, <sup>18</sup>O<sup>16</sup>O, <sup>18</sup>O<sub>2</sub>) were used to determine the overall oxygen exchange rate (R<sub>0</sub>) at each tested temperature. It is further assumed that the oxygen exchange reaction occurs through a 2-step mechanism as proposed by Boukamp et al<sup>41</sup>.



Reaction 2 is the dissociative adsorption oxygen on the surface of the catalyst and reaction 3 is the incorporation of adsorbed oxygen into the oxide lattice. The overall rate for reaction 2 is R<sub>a</sub> and for reaction 3 is R<sub>i</sub>. R<sub>a</sub> and R<sub>i</sub> can be related to R<sub>0</sub> through the equation:

$$\frac{1}{R_0} = \frac{1}{R_a} + \frac{1}{R_i}$$

In Figure 9, the oxygen isotope fractions at different temperatures are plotted for each catalyst. m/z = 32, 34 and 36 corresponds to the three different oxygen species (<sup>16</sup>O<sub>2</sub>, <sup>18</sup>O<sup>16</sup>O, <sup>18</sup>O<sub>2</sub> respectively) present in the pulse. At all temperatures, the un-promoted catalyst has a smaller m/z = 36 fraction than the Na:W = 2:1 redox catalyst, indicating a higher uptake and of <sup>18</sup>O. As the temperature increases, the difference in m/z = 36 fraction becomes greater (97.5% vs. 98.4% at 650°C and 16.5% vs. 69.2% at 850°C). However, the two redox catalysts show opposite behavior with respect to m/z = 32 and 34. At temperatures of 750°C and above, the un-promoted catalyst shows a higher fraction of m/z = 34 than m/z = 32. The increase in m/z = 34 is significant enough at 850°C that it becomes greater than the m/z = 36 fraction. On the Na:W = 2:1 redox catalyst, the

$m/z=32$  fraction is higher than the  $m/z=34$  fraction at all temperatures, and both are always below the  $m/z=36$  fraction. This indicates high oxygen exchange activity and/or mobility on the un-promoted redox catalyst while the NaW promoter inhibits oxygen exchange.

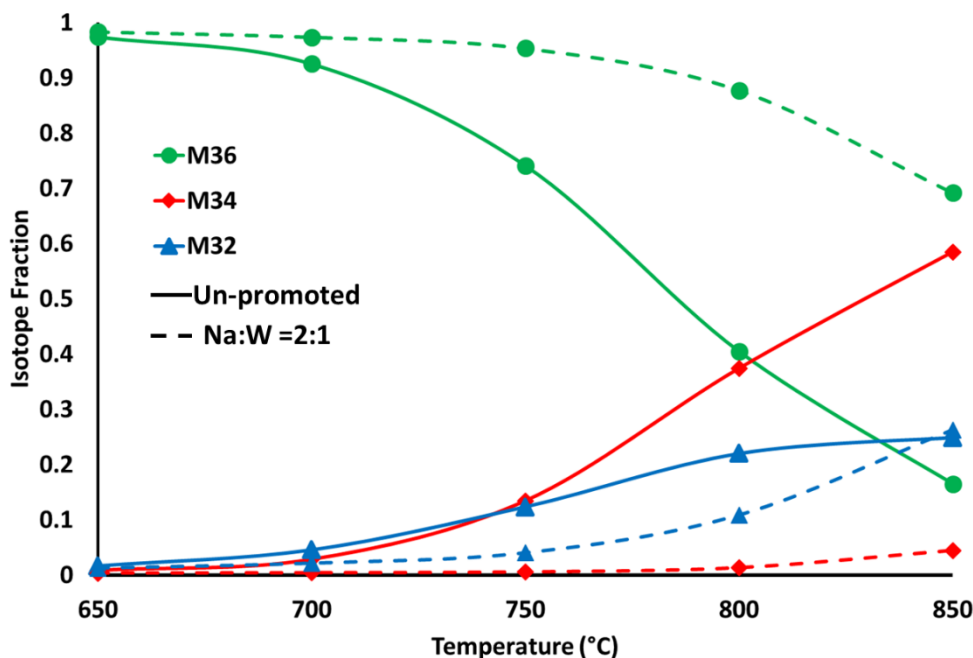
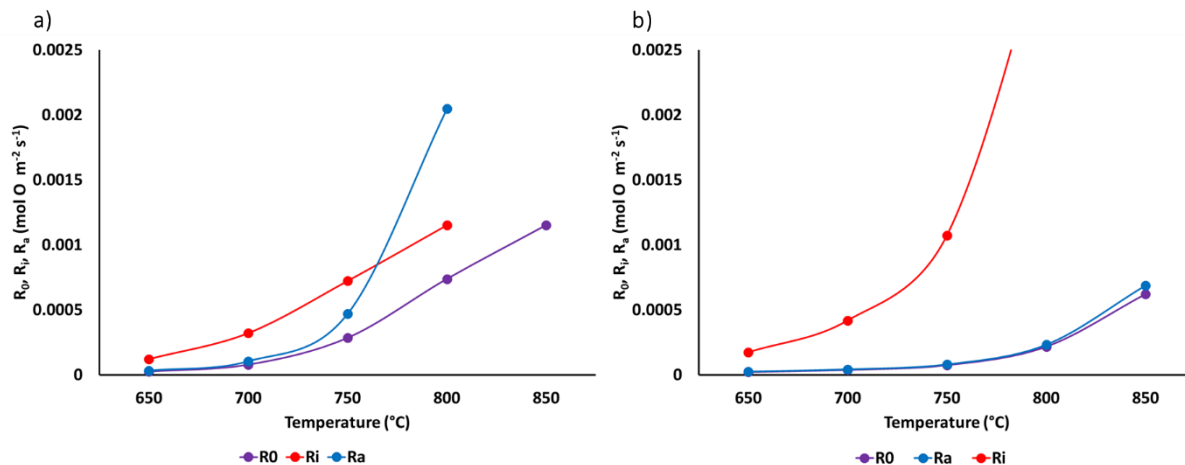


**Figure 9:** Isotope fractions of oxygen species over the un-promoted (solid line) and Na:W = 2:1 (dashed line) redox catalysts at tested temperatures. M32, M34, and M36 correspond to  $^{16}\text{O}_2$ ,  $^{18}\text{O}^{16}\text{O}$ ,  $^{18}\text{O}_2$  respectively.

The calculated rates ( $R_0$ ,  $R_i$ , and  $R_a$ ) are plotted in Figure 10 for the un-promoted and Na:W = 2:1 redox catalysts. At 650 and 700 °C,  $R_0$  is similar on both redox catalysts, but there is a significant increase on the un-promoted redox catalyst at 750 °C while there is not a noticeable increase in  $R_0$  on the Na:W = 2:1 redox catalyst until 800 °C. At all temperatures above 650°C,  $R_0$  is higher on the un-promoted redox catalyst than the Na:W = 2:1 redox catalyst.

When  $R_0$  is further broken down into  $R_a$  and  $R_i$ , significant differences between the un-promoted and Na:W = 2:1 redox catalysts can be observed. On the un-promoted catalyst,  $R_a$  is initially less than  $R_i$  and limits the value of  $R_0$ . As the temperature increases,  $R_i$  increases at a steady rate, but  $R_a$  has a sharper increase at both 750 and 800 °C. At 800°C,  $R_a$  is approximately double the value of  $R_i$ , and is no longer the limiting factor for  $R_0$ .  $R_a$  and  $R_i$  at 850°C cannot be solved, which is likely to be due to the accumulation of exchanged  $^{18}\text{O}$  in the near surface region considering the significantly higher activation energy for  $R_a$  compared to  $R_i$  (Table 1). Near surface accumulation of  $^{18}\text{O}$  would lead to violation of boundary condition in deriving the model.<sup>21,22</sup>

On the Na:W=2:1 redox catalyst,  $R_a$  was lower than  $R_i$  at all measured temperatures. Unlike the un-promoted catalyst, when the temperature was increased to 800 and 850 °C there were significant increases in  $R_i$  instead of  $R_a$ . These increases in  $R_i$  would make it more likely for any disassociated oxygen to be incorporated into the bulk and this is seen in the isotope fraction data which showed a higher fraction of  $m/z = 32$  at these temperatures. It can also be seen that  $R_a$  limits  $R_0$  at all temperatures, keeping  $R_0$  on the Na:W = 2:1 redox catalyst lower than  $R_0$  on the un-promoted redox catalyst. These results indicate that the NaW promoter inhibits oxygen exchange activity on the redox catalyst.



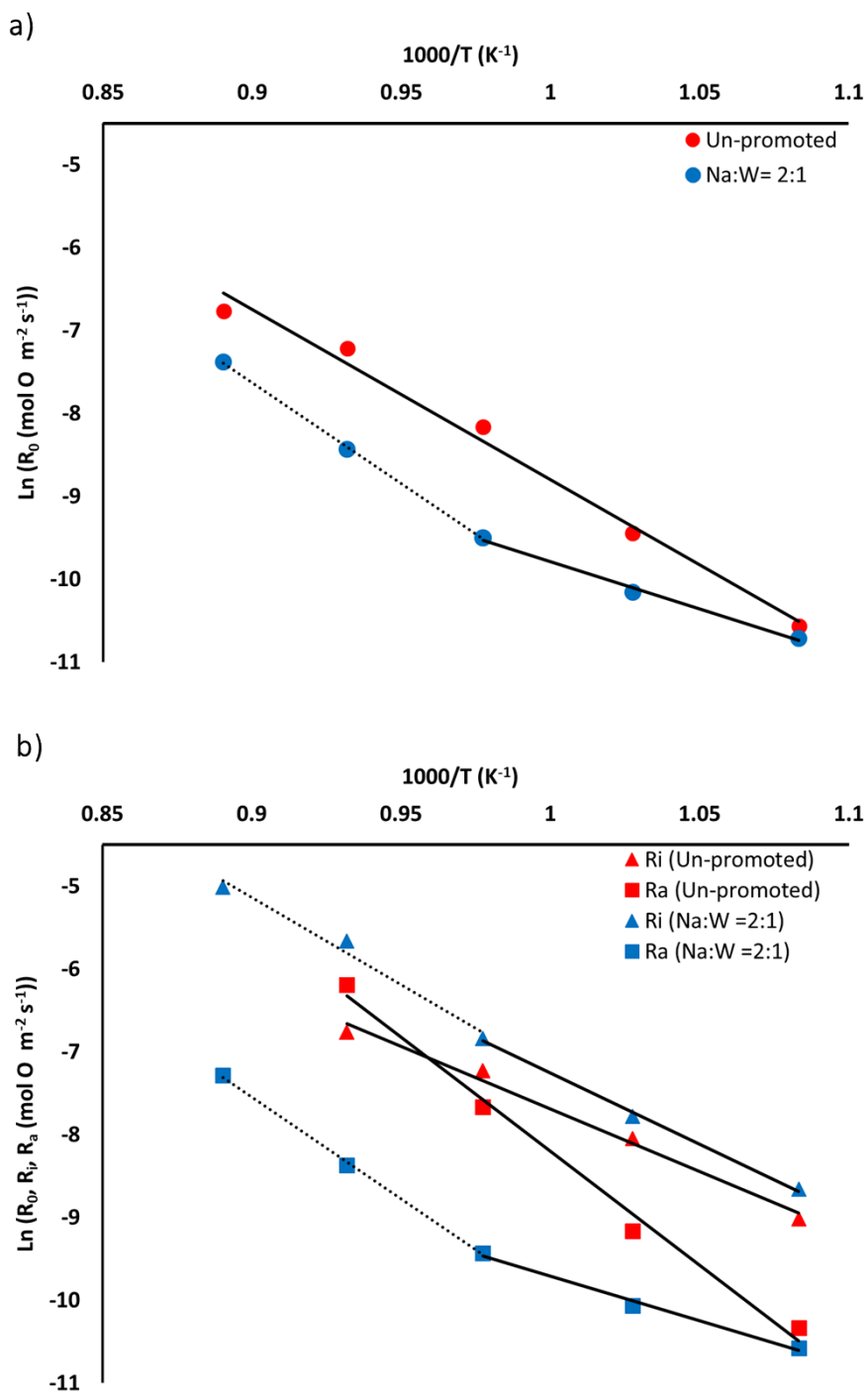
**Figure 10:**  $R_0$ ,  $R_a$ , and  $R_i$  for the a) un-promoted redox catalyst, b) Na:W=2:1 redox catalyst. To maintain identical y-axis scales,  $R_i$  for the Na:W = 2:1 redox catalyst at 800  $^{\circ}\text{C}$  ( $3.5 \cdot 10^{-3} \text{ mol O m}^{-2} \text{ s}^{-1}$ ) and 850  $^{\circ}\text{C}$  ( $6.7 \cdot 10^{-3} \text{ mol O m}^{-2} \text{ s}^{-1}$ ) were not shown in Figure 10b. Full plots can be found in Figure S3

Figure 11 shows the Arrhenius Plots of the reaction rate data. To calculate the activation energies of  $R_0$ ,  $R_i$ , and  $R_a$ , the entire temperature range was used for the un-promoted redox catalyst, but two separate temperature ranges, i.e. below and above 750  $^{\circ}\text{C}$ , were used for the Na:W = 2:1 redox catalyst. The change in slope on the Arrhenius plot is likely due to the melting of the  $\text{Na}_2\text{WO}_4$  promoter. All calculated activation energies are summarized in Table 1. When comparing the un-promoted redox catalyst and the Na:W = 2:1 redox catalyst between 650-750  $^{\circ}\text{C}$ , it can be seen that the un-promoted redox catalyst has higher activation energies and higher or similar pre-exponential factors. At higher temperatures (750-850  $^{\circ}\text{C}$ ), all three activation energies increased for the Na:W = 2:1 redox catalyst, along with significantly increased pre-exponential factors. When comparing the activation energies on the Na:W = 2:1 redox catalyst between 750-850  $^{\circ}\text{C}$  to the activation energies on the un-promoted redox catalyst, it can be seen that the activation energy for  $R_a$  is similar, but  $R_0$  and  $R_i$  are higher on the Na:W = 2:1 redox catalyst. It is also noted that

pre-exponential factor for  $R_a$  is consistently lower on the Na:W=2:1 redox catalyst than the un-promoted redox catalyst which may indicate fewer surface sites for the dissociative adsorption of oxygen. These oxygen exchange experiments show that the NaW surface layer inhibits the overall exchange activity on the redox catalyst by limiting the dissociative adsorption of  $O_2$ . However, the incorporation rate of adsorbed oxygen was promoted by the molten  $Na_2WO_4$  surface layer. Since the typical CL-ODH reactions are carried out at above  $800^\circ C$ , one would anticipate facile  $O^{2-}$  conduction through the molten  $Na_2WO_4$  layer.

**Table 1:** Arrhenius Activation Energies for Un-promoted and Na:W=2:1 redox catalysts

Catalyst	Activation Energy for $R_0$ (KJ/mol)	Pre-Exponential Factor for $R_0$	Activation Energy for $R_i$ (KJ/mol)	Pre-Exponential Factor for $R_i$	Activation Energy for $R_a$ (KJ/mol)	Pre-Exponential Factor for $R_a$
Un-promoted	163.83	11.72	123.82	7.40	227.18	19.27
Na:W=2:1 (650-750°C)	94.94	1.60	143.11	9.93	89.80	1.07
Na:W=2:1 (750-850°C)	202.58	14.28	174.68	13.84	205.04	14.63



**Figure 11:** Arrhenius plots for a)  $R_0$  and b)  $R_a$ , and  $R_i$  for the un-promoted (red) and Na:W=2:1 (blue) redox catalysts. For the Na:W=2:1 redox catalyst, the solid line is for the 650-750°C range and the dashed line is for the 750-850°C range.

## **Probing the CL-ODH Reaction Scheme**

To illustrate the overall reaction scheme for CL-ODH, TPR results on both the un-promoted and NaW promoted redox catalysts using a mixture of hydrogen and ethylene are shown in Figure 12.<sup>42</sup> As can be seen, water formation from hydrogen combustion started at  $\sim 550^\circ\text{C}$  on the un-promoted redox catalyst. In comparison, the NaW promoted redox catalyst is significantly less reducible with an onset temperature of water formation at  $\sim 725^\circ\text{C}$ . This temperature coincides with the onset temperature of ethane thermal cracking. More importantly, negligible  $\text{CO}_x$  formation was observed. Therefore, the NaW promoted redox catalyst is capable of selectively combusting  $\text{H}_2$  generated from thermal cracking of ethane without oxidizing the ethylene product. These results, consistent with our previous studies<sup>12-14</sup>, indicate that CL-ODH proceeds via parallel reactions of i) gaseous ethane cracking to ethylene and hydrogen and ii) selective combustion of hydrogen by lattice oxygen of the NaW promoted redox catalyst.

In addition to the general reaction scheme illustrated above, it would be desirable to obtain additional mechanistic insights on the detailed reaction pathway in view of the redox catalyst's unique  $\text{Mg}_6\text{MnO}_8$ -molten  $\text{Na}_2\text{WO}_4$  core-shell structure. Facile oxidation of the reduced redox catalyst and  $^{18}\text{O}_2$ - $^{16}\text{O}_2$  exchange experiments clearly indicate that oxygen can migrate through the molten  $\text{Na}_2\text{WO}_4$  shell to facilitate the release and uptake of active lattice oxygen from/to the  $\text{Mg}_6\text{MnO}_8$  core in the cyclic redox scheme. The pathway for the oxidation reaction, which involves oxygen incorporation and migration through the molten  $\text{Na}_2\text{WO}_4$  layer to react with the reduced  $\text{Mg}_6\text{MnO}_8$  at the core/shell interface, is relatively straightforward. The selective  $\text{H}_2$  combustion reaction in the CL-ODH step, however, can proceed via one of the following pathways: i)  $\text{H}_2$  reacts, on the outer surface of the redox catalyst, with oxygen diffused from the  $\text{Mg}_6\text{MnO}_8$  core through the molten  $\text{Na}_2\text{WO}_4$  layer; ii)  $\text{H}_2$  dissolves and diffuses through the molten salt, getting

combusted at the  $\text{Na}_2\text{WO}_4/\text{Mg}_6\text{MnO}_8$  interface; iii) combustion of dissolved  $\text{H}_2$  within the molten  $\text{Na}_2\text{WO}_4$  phase. Additional characterizations were performed to determine the detailed mechanism.

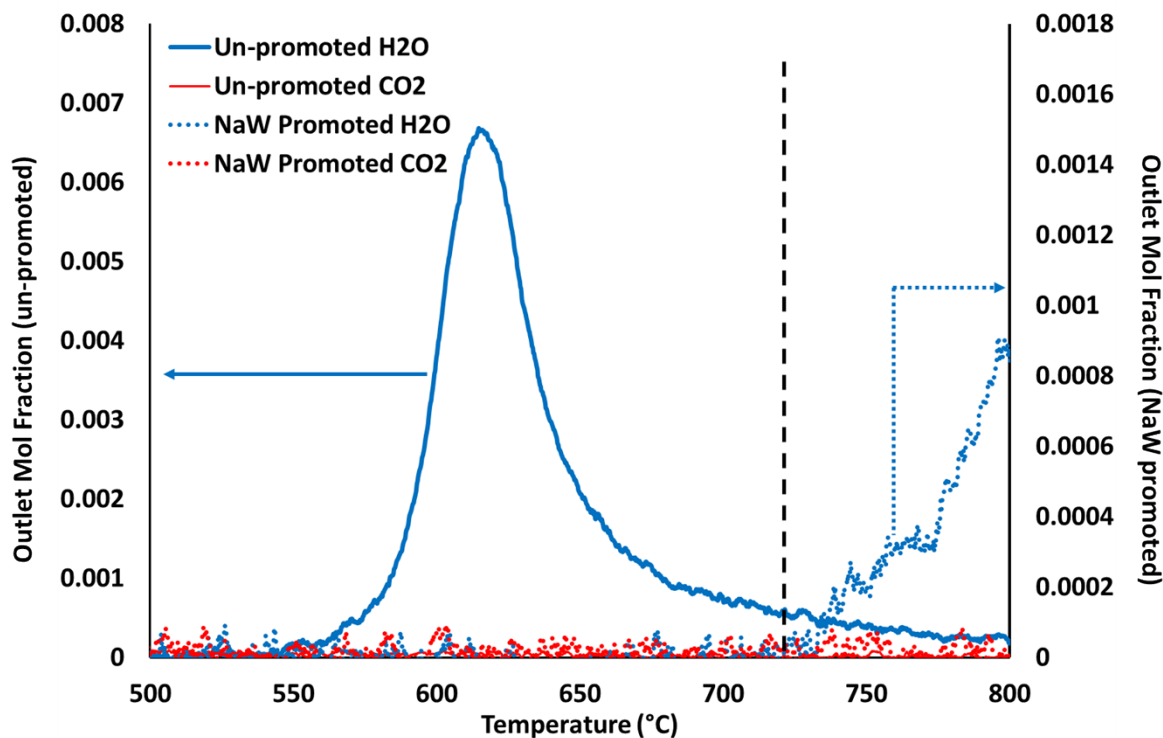


**Figure 12:** 2.5% $\text{H}_2$ /2.5% $\text{C}_2\text{H}_4$  TPR over un-promoted and NaW promoted  $\text{Mg}_6\text{MnO}_8$  catalysts. Vertical dashed line represents the onset temperature for ethane thermal cracking. Total gas flow rate was 100 ml/min,  $\text{H}_2/\text{C}_2\text{H}_4/\text{Ar} = 2.5/2.5/95$ , ramp rate was 5 °C/min.

Previous sections have established that the NaW promoter forms a molten shell around the  $\text{Mg}_6\text{MnO}_8$  redox catalyst that inhibits interaction between  $\text{Mg}_6\text{MnO}_8$  and carbon containing fuels such as  $\text{C}_2\text{H}_6$  and  $\text{CO}$ . In order to test if the oxygen species from the molten layer/redox catalyst are able to activate hydrogen, a  $\text{H}_2\text{-O}_2$  co-feed study was performed at 600 and 700 °C. The results are summarized below in Figure 13.

As expected, the un-promoted redox catalyst shows significantly higher conversion of H<sub>2</sub> than the thermal blank sample, but more significant differences were observed for the Na:W=2:1 redox catalyst. At 600 °C (below the melting temperature), the Na:W=2:1 redox catalyst shows H<sub>2</sub> conversion similar to the thermal blank. However, at 700 °C (above the melting temperature of Na<sub>2</sub>WO<sub>4</sub>), a significantly higher H<sub>2</sub> conversion than the thermal blank was observed. These results indicate that H<sub>2</sub> combustion is facilitated by the melting of the Na<sub>2</sub>WO<sub>4</sub> shell whereas such effects were not observed with CO.

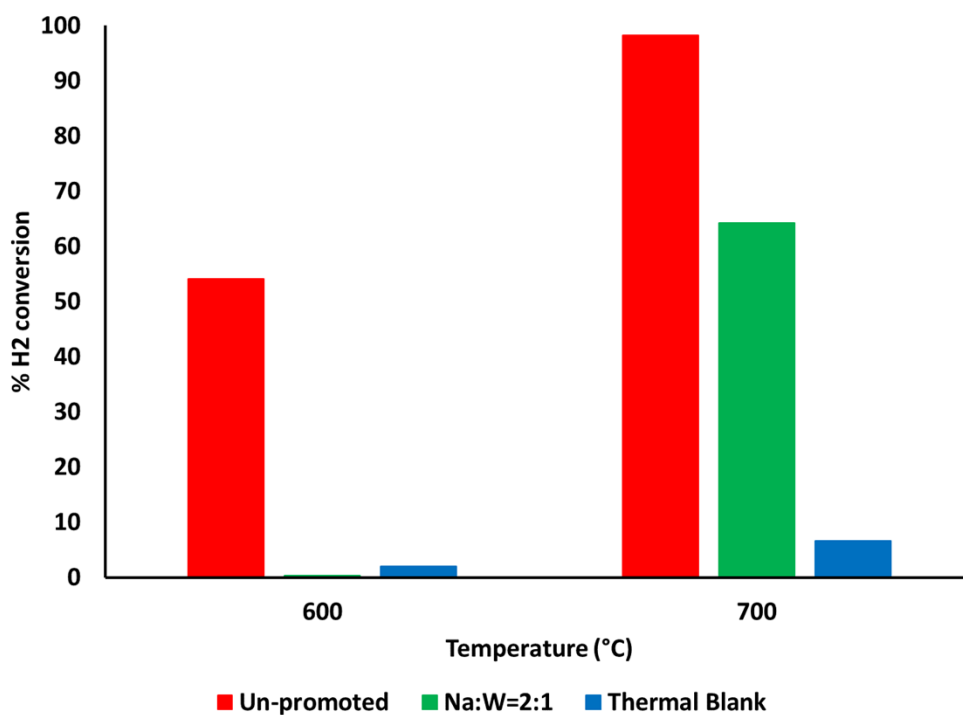


**Figure 13:** Summary of H<sub>2</sub>-O<sub>2</sub> co-feed study. The gas composition was H<sub>2</sub>/O<sub>2</sub>/Ar at a 2/2/96 ratio (vol%).

#### *Solubility of H<sub>2</sub> in the molten NaW promoter*

Given the significantly increased H<sub>2</sub> combustion activity above the Na<sub>2</sub>WO<sub>4</sub> melting temperature, it would be instructive to determine the solubility of H<sub>2</sub> in the molten promoter since

a high solubility of H<sub>2</sub> in molten Na<sub>2</sub>WO<sub>4</sub> would support pathways ii and iii. Gas switching experiments, similar to that reported by Gärtner et. al<sup>43</sup>, were conducted to probe the solubility of H<sub>2</sub>. QMS data from this experiment is shown in Figure 14. The H<sub>2</sub> injection step clearly indicates water formation due to the reduction of Na<sub>2</sub>WO<sub>4</sub>. However, the rate of reduction is rather low ( $4.79 \times 10^{-5}$  mmol O removed/(min-gCatalyst) compared to the average oxygen removal rate of 1.24 mmol O/(min-gCatalyst) for NaW promoted Mg<sub>6</sub>MnO<sub>8</sub> in CL-ODH). This confirms the low reducibility of the Na<sub>2</sub>WO<sub>4</sub> shell, which was further confirmed by *in-situ* Raman experiments (Figure S4). After the H<sub>2</sub> flow was stopped, the water signal started to decrease, but the introduction of O<sub>2</sub> led to a small increase in the water signal before it continued the decreasing trend. Although the small peak indicates potential solubility of H<sub>2</sub>, the rate of water formation from the “dissolved” H<sub>2</sub> was 43 times smaller than rate of water formation during H<sub>2</sub> flow ( $1.10 \times 10^{-6}$  mmol O removed/(min-gCatalyst) vs.  $4.79 \times 10^{-5}$  mmol O removed/(min-gCatalyst)) indicating that the solubility of H<sub>2</sub> in molten Na<sub>2</sub>WO<sub>4</sub> cannot be significant enough to support pathways ii and iii. As such, the likely reaction mechanism is that H<sub>2</sub> is combusted at the surface of the molten Na<sub>2</sub>WO<sub>4</sub> layer by oxygen species from the Mg<sub>6</sub>MnO<sub>8</sub> redox catalyst (pathway i).

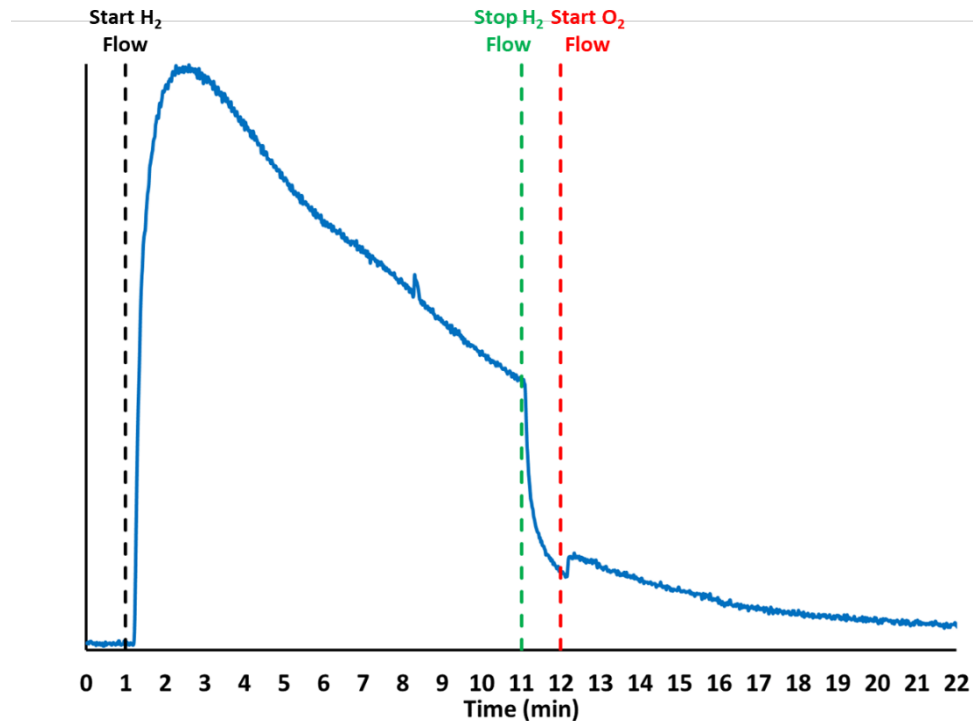


**Figure 14:** Water signal ( $m/z=18$ ) from 15%  $H_2/15\%$   $O_2$  switching experiments over 20wt%  $Na_2WO_4/\alpha-Al_2O_3$  sample at 850 °C. Gas composition over time: 100%Ar(0-1min), 15%  $H_2/Ar$ (1-11min), 100%Ar(11-12min), 15% $O_2/Ar$ (12-22min).

### **Proposed Mechanism**

The extensive characterization results for the  $Na_2WO_4$  promoted  $Mg_6MnO_8$  redox catalyst presented in this paper support a potential CL-ODH mechanism illustrated in Figure 15. At CL-ODH reaction conditions, the  $Na_2WO_4$  promoter forms a molten shell around the  $Mg_6MnO_8$  redox catalyst. During the ethane ODH step, ethane undergoes thermal cracking in the gas phase to form ethylene and hydrogen. Next, the formed hydrogen is combusted to water at the gas-molten  $Na_2WO_4$  interface. This combustion does not occur in the molten layer or at the molten  $Na_2WO_4$ - $Mg_6MnO_8$  interface as the solubility of hydrogen in molten  $Na_2WO_4$  is too low to support such a reaction pathway. Rather, hydrogen is combusted by the molten  $Na_2WO_4$  via a redox mechanism. During this reduction, the  $WO_4^{2-}$  anion can be reduced to  $WO_3^-$  anion (as reported in sodium

tungsten bronze formation ( $\text{Na}_x\text{WO}_3$ ,  $x \leq 1.44$ ). The  $\text{WO}_3^-$  anion is re-oxidized to  $\text{WO}_4^{2-}$  with lattice oxygen from the  $\text{Mg}_6\text{MnO}_8$  redox catalyst so that further hydrogen combustion can occur. It is noted that such a redox mechanism would require electron conduction through the molten layer. Considering the high electronic conductivity well-documented for tungsten bronze<sup>45</sup>, such a pathway would be feasible. The redox nature of molten  $\text{Na}_2\text{WO}_4$  was further validated in experiments utilizing sharp  $^{18}\text{O}_2$  pulses during a broad  $\text{H}_2$  pulse (see supporting information file). As such, the  $\text{Na}_2\text{WO}_4$  promoter serves multiple functions in terms of: i. forming a molten shell on  $\text{Mg}_6\text{MnO}_8$  to inhibit hydrocarbon combustion; ii. facilitating oxygen exchange at the interfaces of the gas-molten salt and molten salt- $\text{Mg}_6\text{MnO}_8$  via a redox mechanism ( $\text{WO}_4^{2-} \leftrightarrow \text{WO}_3^-$ ); iii. transporting the exchanged oxygen (and electrons) from/to the  $\text{Mg}_6\text{MnO}_8$  core during the CL-ODH and re-oxidation steps.

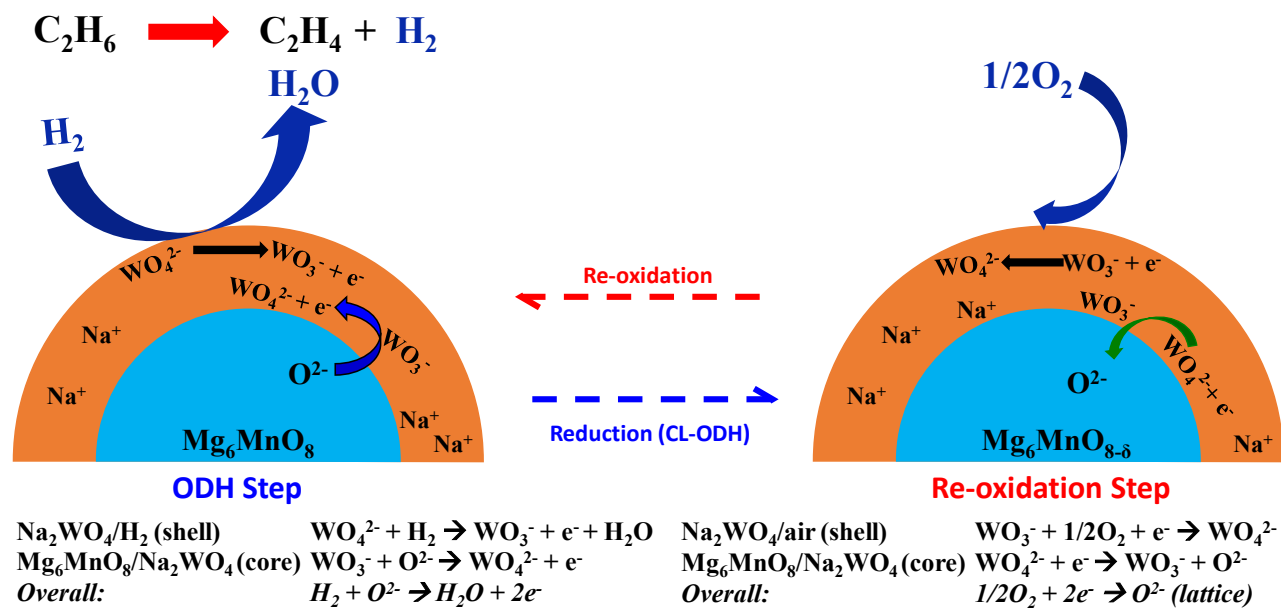


**Figure 15:** Proposed mechanism of CL-ODH of ethane over NaW-promoted  $\text{Mg}_6\text{MnO}_8$  redox catalysts (The electrons in each step are balanced by the reduction or oxidation of the Mn cations in the  $\text{Mg}_6\text{MnO}_8$  core. This is not shown in the graph for simplicity).

## Conclusion

The current study investigates the effect of sodium and tungsten promoters on  $\text{Mg}_6\text{MnO}_8$  based redox catalysts for chemical looping-ODH of ethane. By varying the ratio of Na and W, it was determined that, in order to optimize ethylene yield, there needs to be a balance between the relative amount of Na and W. W is important to retain Na on the surface of the redox catalyst. However, if the Na:W is lowered to significantly below 2:1 (the stoichiometric ratio of  $\text{Na}_2\text{WO}_4$ ), mixed tungsten oxide phases other than  $\text{Na}_2\text{WO}_4$  will form, resulting in increased  $\text{CO}_x$  formation. Surface characterization indicates that the NaW promoter forms a molten shell around the  $\text{Mg}_6\text{MnO}_8$  redox catalyst under the CL-ODH operating conditions. Methanol TPSR and *in-situ* DRIFTS experiments indicate that the NaW promoter inhibits the activation of reactant molecules on the surface of the catalyst by significantly suppressing the number of basic sites on redox catalyst.  $^{18}\text{O}$ - $^{16}\text{O}$  exchange experiments reveal that the NaW promoter also inhibits the dissociative adsorption of oxygen and decreases the rate of oxygen exchange.  $\text{O}_2$  co-feed studies indicate that, when the  $\text{Na}_2\text{WO}_4$  promoter is in a solid phase,  $\text{H}_2$  and CO conversions are both inhibited. Melting of the  $\text{Na}_2\text{WO}_4$  shell at  $\sim 694$  °C, however, lead to significantly increased  $\text{H}_2$  combustion activity whereas combustion of CO and hydrocarbons are still inhibited. The ability to selectively combust  $\text{H}_2$  is important since the CL-ODH reaction in the presence of  $\text{Na}_2\text{WO}_4$  promoted  $\text{Mg}_6\text{MnO}_8$  proceeds via gas phase cracking in parallel with selective combustion of hydrogen by the redox catalyst. Further characterizations of  $\text{H}_2$  solubility in  $\text{Na}_2\text{WO}_4$ ,  $^{18}\text{O}_2$  exchange behavior, and surface redox sites indicate that  $\text{H}_2$  is primarily combusted at the gas- $\text{Na}_2\text{WO}_4$  molten shell interface via redox reactions of the tungsten salt, most likely between the  $\text{WO}_4^{2-}$  (tungstate) and  $\text{WO}_3^-$  (tungsten bronze). Therefore, the molten  $\text{Na}_2\text{WO}_4$  layer plays critical roles in: i. decreasing the number of basic sites and non-selective oxygen species on  $\text{Mg}_6\text{MnO}_8$ ; ii. facilitating the

exchange and transport of lattice oxygen from/to the  $\text{Mg}_6\text{MnO}_8$  core for selective hydrogen combustion via redox reactions of tungsten salt. This detailed understanding of the functions of the  $\text{Na}_2\text{WO}_4$  promoter and the reaction pathway can guide the design and further optimization of CL-ODH redox catalysts for ethylene production with significantly reduced energy consumptions and  $\text{CO}_2$  emissions.

### **Supporting Information**

The Supporting Information is available free of charge on the ACS Publications website Rietveld Refinement, DSC measurements of Na:W = 2:1 redox catalyst, Reaction rates for  $^{18}\text{O}$ - $^{16}\text{O}$  exchange experiments, and *In-situ* Raman experiments at ORNL, redox nature of  $\text{Na}_2\text{WO}_4$ ,  $\text{C}_2\text{H}_4$ - $\text{O}_2$  co-feed experiments, and comparison of un-promoted and Na:W = 2:1 redox catalysts.

### **Acknowledgements**

This work was supported by the U.S. National Science Foundation (Award No. CBET-1604605), the US Department of Energy (RAPID Subaward DE-EE0007888-05-6), and the Kenan Institute for Engineering, Technology and Science at NC State University. The authors acknowledge the use of the Analytical Instrumentation Facility (AIF) at North Carolina State University, which is supported by the State of North Carolina and the National Science Foundation. ZB and ZW were supported by the U.S. Department of Energy, Office of Science, Office of Basic Energy Sciences, Chemical Sciences, Geosciences, and Biosciences Division. Part of the work including *in situ* Raman was conducted at the Center for Nanophase Materials Sciences, which is a DOE Office of Science User Facility.

### **References**

- (1) *Ullmann's Encyclopedia of Industrial Chemistry*; Wiley-VCH Verlag GmbH & Co. KGaA: Weinheim, Germany, 2000.

- (2) Sattler, J. J. H. B.; Ruiz-Martinez, J.; Santillan-Jimenez, E.; Weckhuysen, B. M. Catalytic Dehydrogenation of Light Alkanes on Metals and Metal Oxides. *Chem. Rev.* **2014**, *114*, 10613–10653.
- (3) Oglend, A.; Lindbäck, M. E.; Osmundsen, P. Shale Gas Boom Affecting the Relationship Between LPG and Oil Prices. *Energy J.* **2015**, *36*.
- (4) Ren, T.; Patel, M.; Blok, K. Olefins from Conventional and Heavy Feedstocks: Energy Use in Steam Cracking and Alternative Processes. *Energy* **2006**, *31*, 425–451.
- (5) Gärtner, C. A.; van Veen, A. C.; Lercher, J. A. Oxidative Dehydrogenation of Ethane: Common Principles and Mechanistic Aspects. *ChemCatChem* **2013**, *5*, 3196–3217.
- (6) Bhasin, M. M. Is True Ethane Oxydehydrogenation Feasible? *Top. Catal.* **2003**, *23*, 145–149.
- (7) Burch, R.; Swarnakar, R. Oxidative Dehydrogenation of Ethane on Vanadium-Molybdenum Oxide and Vanadium-Niobium-Molybdenum Oxide Catalysts. *Appl. Catal.* **1991**, *70*, 129–148.
- (8) Mamedov, E. A.; Cortés Corberán, V. Oxidative Dehydrogenation of Lower Alkanes on Vanadium Oxide-Based Catalysts. The Present State of the Art and Outlooks. *Appl. Catal. A Gen.* **1995**, *127*, 1–40.
- (9) Bañares, M. A. Supported Metal Oxide and Other Catalysts for Ethane Conversion: A Review. *Catal. Today* **1999**, *51*, 319–348.
- (10) Gaab, S.; Find, J.; Müller, T. E.; Lercher, J. A. Kinetics and Mechanism of the Oxidative Dehydrogenation of Ethane over Li/Dy/Mg/O/(Cl) Mixed Oxide Catalysts. *Top. Catal.* **2007**, *46*, 101–110.
- (11) Haribal, V. P.; Neal, L. M.; Li, F. Oxidative Dehydrogenation of Ethane under a Cyclic

- Redox Scheme – Process Simulations and Analysis. *Energy* **2017**, *119*, 1024–1035.
- (12) Yusuf, S.; Neal, L. M.; Li, F. Effect of Promoters on Manganese-Containing Mixed Metal Oxides for Oxidative Dehydrogenation of Ethane via a Cyclic Redox Scheme. *ACS Catal.* **2017**, *7*, 5163–5173.
- (13) Neal, L. M.; Yusuf, S.; Sofranko, J. A.; Li, F. Oxidative Dehydrogenation of Ethane: A Chemical Looping Approach. *Energy Technol.* **2016**, *4*, 1200–1208.
- (14) Yusuf, S.; Neal, L.; Haribal, V.; Baldwin, M.; Lamb, H. H.; Li, F. Manganese Silicate Based Redox Catalysts for Greener Ethylene Production via Chemical Looping – Oxidative Dehydrogenation of Ethane. *Appl. Catal. B Environ.* **2018**, *232*, 77–85.
- (15) Gao, Y.; Neal, L. M.; Li, F. Li-Promoted  $\text{La}_x\text{Sr}_{2-x}\text{XFeO}_{4-\delta}$  Core-Shell Redox Catalysts for Oxidative Dehydrogenation of Ethane under a Cyclic Redox Scheme. *ACS Catal.* **2016**, *6*, 7293–7302.
- (16) Gao, Y.; Haeri, F.; He, F.; Li, F. Alkali Metal-Promoted  $\text{La}_x\text{Sr}_{2-x}\text{FeO}_{4-\delta}$  Redox Catalysts for Chemical Looping Oxidative Dehydrogenation of Ethane. *ACS Catal.* **2018**, *8*, 1757–1766.
- (17) Galinsky, N.; Mishra, A.; Zhang, J.; Li, F.  $\text{Ca}_{1-x}\text{A}_x\text{MnO}_3$  (A=Sr and Ba) Perovskite Based Oxygen Carriers for Chemical Looping with Oxygen Uncoupling (CLOU). *Appl. Energy* **2015**, *157*, 358–367.
- (18) Galinsky, N.; Sendi, M.; Bowers, L.; Li, F.  $\text{CaMn}_{1-x}\text{B}_x\text{O}_{3-\delta}$  (B = Al, V, Fe, Co, and Ni) Perovskite Based Oxygen Carriers for Chemical Looping with Oxygen Uncoupling (CLOU). *Appl. Energy* **2016**, *174*, 80–87.
- (19) Shafiearhood, A.; Stewart, A.; Li, F. Iron-Containing Mixed-Oxide Composites as Oxygen Carriers for Chemical Looping with Oxygen Uncoupling (CLOU). *Fuel* **2015**,

139, 1–10.

- (20) Galinsky, N. L.; Shafiefarhood, A.; Chen, Y.; Neal, L.; Li, F. Effect of Support on Redox Stability of Iron Oxide for Chemical Looping Conversion of Methane. *Appl. Catal. B Environ.* **2015**, *164*, 371–379.
- (21) He, F.; Li, F. Perovskite Promoted Iron Oxide for Hybrid Water-Splitting and Syngas Generation with Exceptional Conversion. *Energy Environ. Sci.* **2015**, *8*, 535–539.
- (22) Luo, S.; Zeng, L.; Xu, D.; Kathe, M.; Chung, E.; Deshpande, N.; Qin, L.; Majumder, A.; Hsieh, T.-L.; Tong, A.; et al. Shale Gas-to-Syngas Chemical Looping Process for Stable Shale Gas Conversion to High Purity Syngas with a H<sub>2</sub> : CO Ratio of 2 : 1. *Energy Environ. Sci.* **2014**, *7*, 4104–4117.
- (23) Lim, H. S.; Kang, D.; Lee, J. W. Phase Transition of Fe<sub>2</sub>O<sub>3</sub>–NiO to NiFe<sub>2</sub>O<sub>4</sub> in Perovskite Catalytic Particles for Enhanced Methane Chemical Looping Reforming- Decomposition with CO<sub>2</sub> Conversion. *Appl. Catal. B Environ.* **2017**, *202*, 175–183.
- (24) Kang, D.; Lim, H. S.; Lee, M.; Lee, J. W. Syngas Production on a Ni-Enhanced Fe<sub>2</sub>O<sub>3</sub>/Al<sub>2</sub>O<sub>3</sub> Oxygen Carrier via Chemical Looping Partial Oxidation with Dry Reforming of Methane. *Appl. Energy* **2018**, *211*, 174–186.
- (25) Al-Ghamdi, S.; Volpe, M.; Hossain, M. M.; de Lasa, H. VO<sub>x</sub>/c-Al<sub>2</sub>O<sub>3</sub> Catalyst for Oxidative Dehydrogenation of Ethane to Ethylene: Desorption Kinetics and Catalytic Activity. *Appl. Catal. A Gen.* **2013**, *450*, 120–130.
- (26) Elbadawi, A. H.; Ba-Shammakh, M. S.; Al-Ghamdi, S.; Razzak, S. A.; Hossain, M. M. Reduction Kinetics and Catalytic Activity of VO<sub>x</sub>/γ-Al<sub>2</sub>O<sub>3</sub>-ZrO<sub>2</sub> for Gas Phase Oxygen Free ODH of Ethane. *Chem. Eng. J.* **2016**, *284*, 448–457.
- (27) Jones, C. A.; Leonard, J. J.; Sofranko, J. A. The Oxidative Conversion of Methane to

- Higher Hydrocarbons over Alkali-Promoted MnSiO<sub>2</sub>. *J. Catal.* **1987**, *103* (2), 311–319.
- (28) Sofranko, J. A.; Leonard, J. J.; Jones, C. A.; Gaffney, A. M.; Withers, H. P. Catalytic Oxidative Coupling of Methane over Sodium-Promoted Mn/SiO<sub>2</sub> and Mn/MgO. *Catal. Today* **1988**, *3*, 127–135.
- (29) Bouwmeester, H. J. M.; Song, C.; Zhu, J.; Yi, J.; van Sint Annaland, M.; Boukamp, B. A. A Novel Pulse Isotopic Exchange Technique for Rapid Determination of the Oxygen Surface Exchange Rate of Oxide Ion Conductors. *Phys. Chem. Chem. Phys.* **2009**, *11*, 9640-9643.
- (30) Yoo, C.-Y.; Bouwmeester, H. J. M. Oxygen Surface Exchange Kinetics of SrTi<sub>1-x</sub>Fe<sub>x</sub>O<sub>3-δ</sub> Mixed Conducting Oxides. *Phys. Chem. Chem. Phys.* **2012**, *14*, 11759-11765.
- (31) Wachs, I. E.; Routray, K. Catalysis Science of Bulk Mixed Oxides. *ACS Catal.* **2012**, *2*, 1235–1246.
- (32) Badlani, M.; Wachs, I. E. Methanol: A “Smart” Chemical Probe Molecule. *Catal. Letters* **2001**, *75*, 137–149.
- (33) Botha, A.; Strydom, C. A. DTA and FT-IR Analysis of the Rehydration of Basic Magnesium Carbonate. *J. Therm. Anal. Calorim.* **2003**, *71*, 987–996.
- (34) Zhiping Zhang, †; Yajun Zheng, ‡; Yuwen Ni, †; Zhongmin Liu, †; Jiping Chen, \*, † and Liang†, X. Temperature- and PH-Dependent Morphology and FT–IR Analysis of Magnesium Carbonate Hydrates. **2006**, *110*, 12969-12973.
- (35) Einaga, H.; Futamura, S. Catalytic Oxidation of Benzene with Ozone over Alumina-Supported Manganese Oxides. *J. Catal.* **2004**, *227*, 304–312.
- (36) Cabilla, G. C.; Bonivardi, A. L.; Baltanás, M. A. Infrared Study of the Adsorption of

- Formic Acid on Clean and Ca-Promoted Pd/SiO<sub>2</sub> Catalysts. *Appl. Catal. A Gen.* **2003**, 255, 181–195.
- (37) Millar, G. J.; Rochester, C. H.; Waugh, K. C. An FTIR Study of the Adsorption of Formic Acid and Formaldehyde on Potassium-Promoted Cu/SiO<sub>2</sub> Catalysts. *J. Catal.* **1995**, 155, 52–58.
- (38) Boccuzzi, F.; Chiorino, A.; Manzoli, M. FTIR Study of Methanol Decomposition on Gold Catalyst for Fuel Cells. *J. Power Sources* **2003**, 118, 304–310.
- (39) Kähler, K.; Holz, M. C.; Rohe, M.; Strunk, J.; Muhler, M. Probing the Reactivity of ZnO and Au/ZnO Nanoparticles by Methanol Adsorption: A TPD and DRIFTS Study. *ChemPhysChem* **2010**, 11, 2521–2529.
- (40) Kuhn, J. N.; Ozkan, U. S. Surface Properties of Sr- and Co-Doped LaFeO<sub>3</sub>. *J. Catal.* **2008**, 253, 200–211.
- (41) Boukamp, B. A.; van Hassel, B. A.; Vinke, I. C.; De Vries, K. J.; Burggraaf, A. J. The Oxygen Transfer Process on Solid Oxide/Noble Metal Electrodes, Studied with Impedance Spectroscopy, Dc Polarization and Isotope Exchange. *Electrochim. Acta* **1993**, 38, 1817–1825.
- (42) Dudek, R. B.; Gao, Y.; Zhang, J.; Li, F. Manganese-Containing Redox Catalysts for Selective Hydrogen Combustion under a Cyclic Redox Scheme. *AIChE J.* **2018**, 64, 3141–3150.
- (43) Gärtner, C. A.; van Veen, A. C.; Lercher, J. A. Oxidative Dehydrogenation of Ethane on Dynamically Rearranging Supported Chloride Catalysts. *J. Am. Chem. Soc.* **2014**, 136, 12691–12701.
- (44) Mann, M.; Shter, G. E.; Reisner, G. M.; Grader, G. S. Synthesis of Tungsten Bronze

Powder and Determination of Its Composition. *J. Mater. Sci.* **2007**, *42*, 1010–1018.

- (45) Brown, B. W.; Banks, E. The Sodium Tungsten Bronzes. *J. Am. Chem. Soc.* **1954**, *76*, 963–966.

**Effects of Sodium and Tungsten Promoters on  $\text{Mg}_6\text{MnO}_8$  Based Core-Shell Redox Catalysts for Chemical Looping – Oxidative Dehydrogenation of Ethane**

**Seif Yusuf<sup>1</sup>, Luke Neal<sup>1</sup>, Zhenghong Bao<sup>2</sup>, Zili Wu<sup>2</sup>, and Fanxing Li<sup>1\*</sup>**

<sup>1</sup> Department of Chemical and Biomolecular Engineering, North Carolina State University, 911 Partners Way, Raleigh, North Carolina, 27695-7905, United States.

<sup>2</sup> Center for Nanophase Materials Sciences and Chemical Science Division, Oak Ridge National Laboratory, Oak Ridge, Tennessee 37831, United States

\* Corresponding author. Email: [fli5@ncsu.edu](mailto:fli5@ncsu.edu)

**Rietveld Refinement**

The XRD pattern for Rietveld refinement was collected on a PANalytical Empyrean diffractometer under  $\text{CuK}_\alpha$  radiation from a sealed tube generator at 45kV and 40mA, with PIXcel1D detector at room temperature. Measurement was taken under Bragg-Brentano configuration using a spinning sample stage at  $0.01^\circ$  step size and 4.5s per step. Data was analyzed and refined using GSAS-II software package<sup>1</sup>.

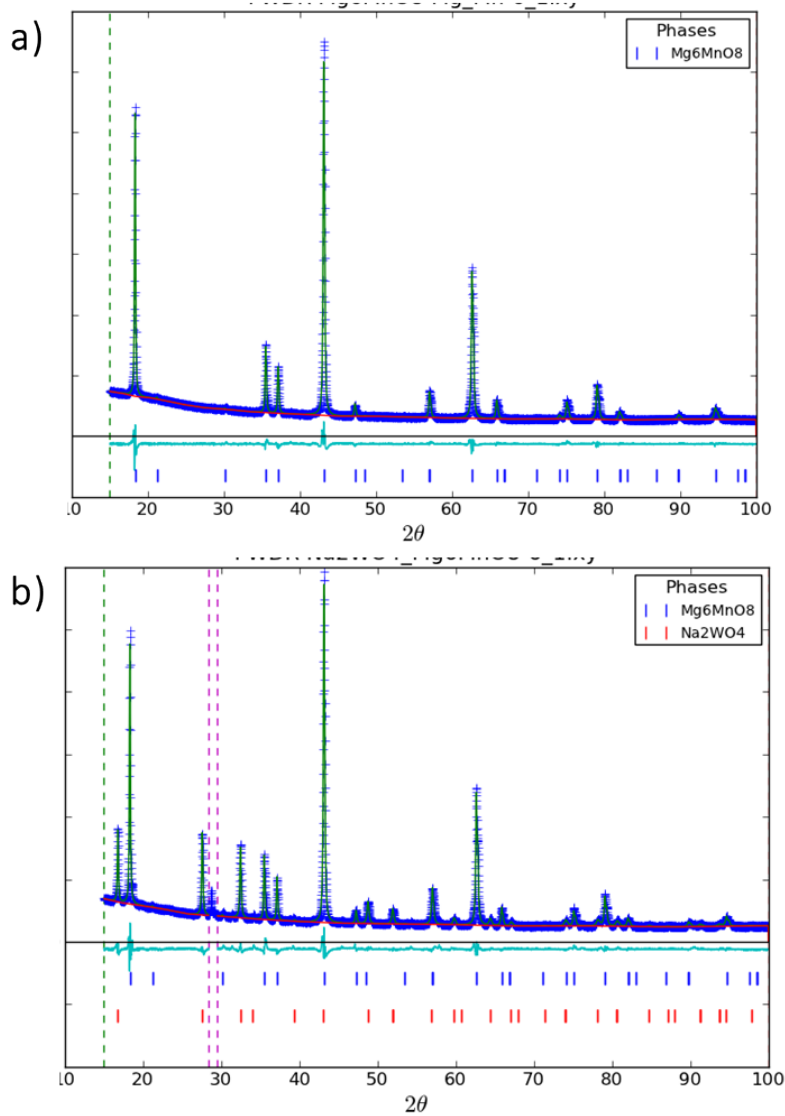


**Figure S1:** Reitveld Refinement fits of a) un-promoted  $\text{Mg}_6\text{MnO}_8$  and b) Na:W=2:1 promoted  $\text{Mg}_6\text{MnO}_8$  redox catalysts

**Table S1:** Refinement Results

Sample	Mg <sub>6</sub> MnO <sub>8</sub>	Na <sub>2</sub> WO <sub>4</sub> -Mg <sub>6</sub> MnO <sub>8</sub>	
Phase	Mg <sub>6</sub> MnO <sub>8</sub>	Mg <sub>6</sub> MnO <sub>8</sub>	Na <sub>2</sub> WO <sub>4</sub>
Phase Fraction	1	0.9588	0.0412
Z	4	4	8
Space group	Fm-3m	Fm-3m	Fd-3m
a	8.38337	8.383307	9.14453
V	589.191	589.127	764.688
wR	0.033	0.052	

**DSC Measurement**

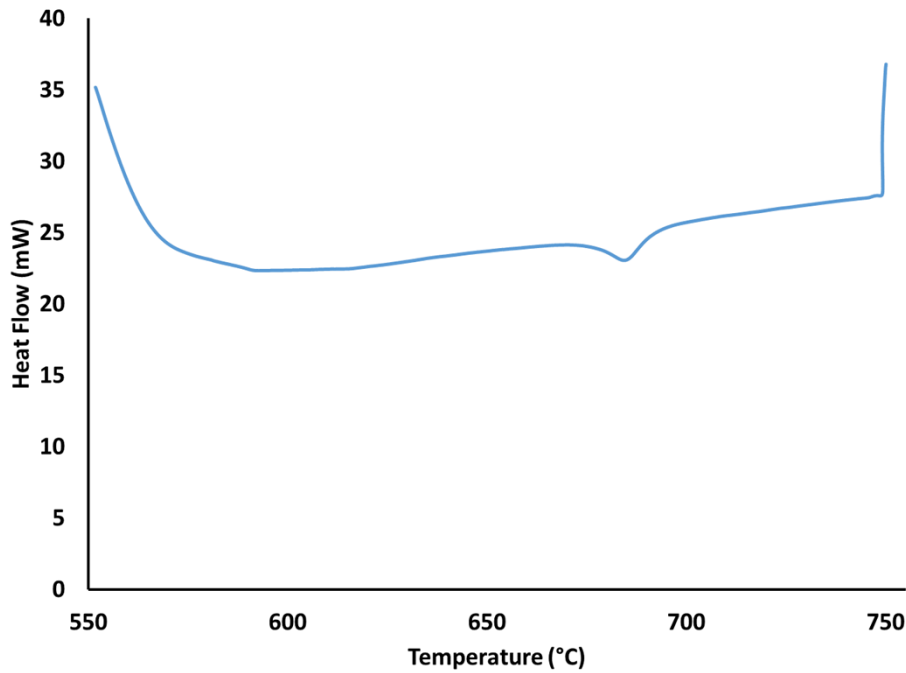


**Figure S2:** DSC measurements over Na:W=2:1 redox catalyst

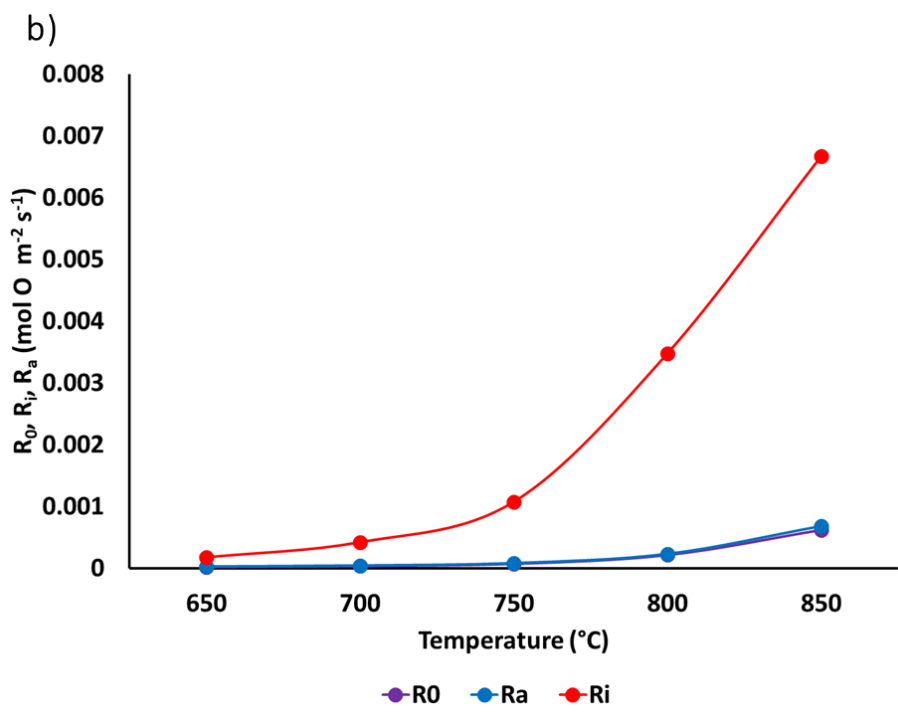
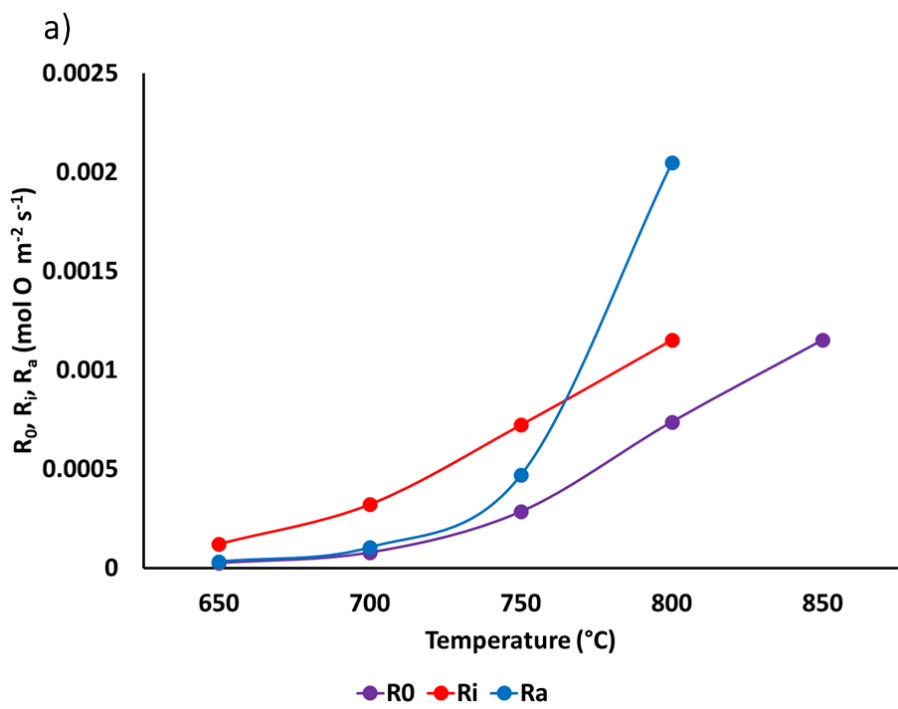


**Figure S3:** Full plots of  $R_0$ ,  $R_a$ , and  $R_i$  for the a) un-promoted redox catalyst, b) Na:W=2:1 redox catalyst.

## **In-situ Raman Spectroscopy**

### **Experimental Details**

*In-situ* Raman spectroscopy measurements were performed at Oak Ridge National Laboratory on the a 20wt% Na<sub>2</sub>WO<sub>4</sub>/α-Al<sub>2</sub>O<sub>3</sub> sample in a Linkam CCR1000 reactor using excitation from a HeCd laser (Melles Griot) at 442 nm (5 mW at sample position). After the sample was loaded into the sample chamber, it was heated to 850°C in 10% O<sub>2</sub>/Ar (30mL/min). The temperature was held at 850°C throughout the following steps. Next, the sample chamber was purged with 100% Ar for 10 minutes and then the flow was switched to 4% H<sub>2</sub>/Ar. After 1 hour, the sample chamber was purged with 100% Ar and then the flow was switched back to 10%O<sub>2</sub> for 10 minutes before the sample chamber was cooled. Raman spectra were taken throughout the experiment and the results are summarized in Figure S4.

The Raman spectra were normalized to the highest peak at ~ 400 cm<sup>-1</sup> and no significant changes can be seen during the experiment in both O<sub>2</sub> and H<sub>2</sub> atmosphere. This indicates that there is no bulk reduction of Na<sub>2</sub>WO<sub>4</sub> by H<sub>2</sub> at the typical reaction temperature of 850°C.

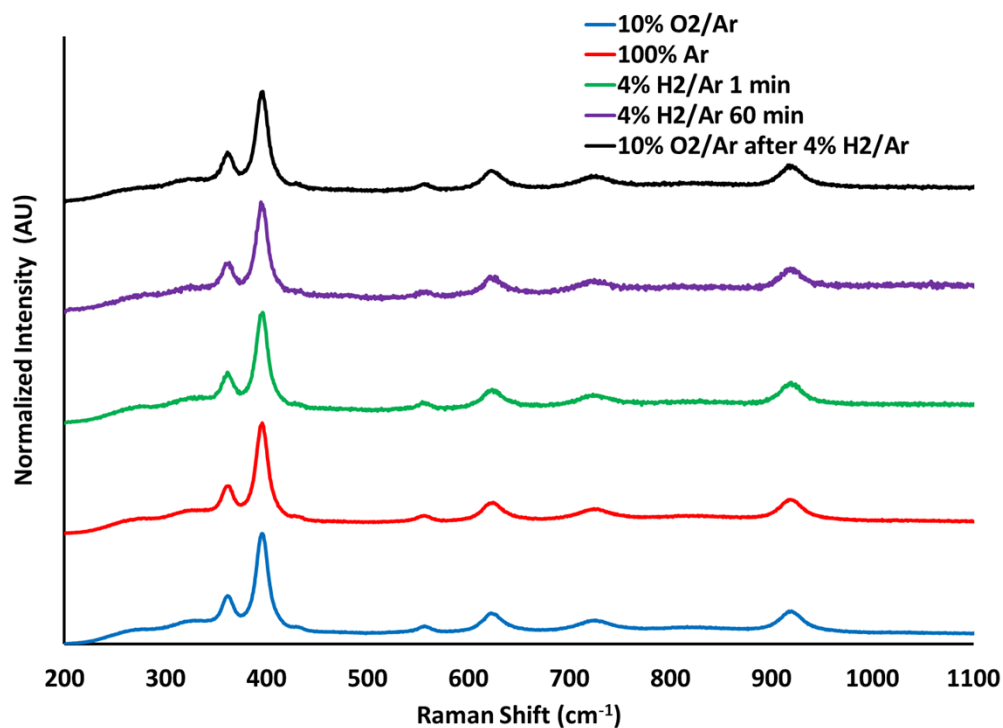


**Figure S4:** Raman spectra of 20wt%Na<sub>2</sub>WO<sub>4</sub>/Al<sub>2</sub>O<sub>3</sub> during *in-situ* experiments at 850°C. All spectra were collected at 850 °C and normalized from 0 to 1.

## Redox Nature of Na<sub>2</sub>WO<sub>4</sub>

### Experimental Details

In order to test the redox nature of Na<sub>2</sub>WO<sub>4</sub>, a 20wt% Na<sub>2</sub>WO<sub>4</sub>/α-Al<sub>2</sub>O<sub>3</sub> sample was synthesized. The synthesis was done with the same procedure as described for the redox catalysts. Sodium tungstate dihydrate was used as the precursor for Na<sub>2</sub>WO<sub>4</sub> and the Al grit used to pack reactor U-tubes was used as the α-Al<sub>2</sub>O<sub>3</sub> material. After mixing sodium tungstate dihydrate dissolved in water with α-Al<sub>2</sub>O<sub>3</sub>, the sample was dried overnight at 80°C and calcined in air at 450°C for 3 hours and then at 900°C for 8 hours.

The test to determine the redox nature of Na<sub>2</sub>WO<sub>4</sub> utilized a broad pulse of H<sub>2</sub> and a sharp pulse <sup>18</sup>O with helium as a carrier gas. 5g of the 20 wt% Na<sub>2</sub>WO<sub>4</sub>/α-Al<sub>2</sub>O<sub>3</sub> sample (1g of Na<sub>2</sub>WO<sub>4</sub>

total) was then loaded into a quartz U-tube reactor and packed with un-promoted Al grit on either side. The U-tube was then loaded into the reactor and 60 sccm of He was flown to purge any oxygen. Then a six-way valve was used to inject a 1ml pulse of 100% H<sub>2</sub> into the reactor. Before entering the reactor, the pulse was broadened by flowing through an empty vessel. When the peak of the H<sub>2</sub> pulse was reached, a sharp 0.1mL of <sup>18</sup>O (33% in He) was injected into the reactor. A QMS was used to analyze the products formed during the experiment. For comparison, experiments with an Ar pulse instead of <sup>18</sup>O and an experiment with only a broad H<sub>2</sub> pulse were run. The experiment took place at 850°C and a room temperature run was used for reference. A blank sample (only Al grit) was also run for comparison at the same conditions as the 20 wt% Na<sub>2</sub>WO<sub>4</sub>/α-Al<sub>2</sub>O<sub>3</sub> sample.

## Results

In Figure S5, a comparison of the blank and the 20 wt% Na<sub>2</sub>WO<sub>4</sub>/α-Al<sub>2</sub>O<sub>3</sub> at 850°C with a broad H<sub>2</sub> pulse and a sharp <sup>18</sup>O<sub>2</sub> pulses can be seen. On m/z= 18 of the 20 wt% Na<sub>2</sub>WO<sub>4</sub>/α-Al<sub>2</sub>O<sub>3</sub> sample, a sharp peak followed by a broad peak can be seen. The sharp peak is due to injection of <sup>18</sup>O<sub>2</sub> (<sup>18</sup>O fragment) as no sharp pulse can be seen of m/z= 17, which would have been solely associated with H<sub>2</sub><sup>16</sup>O. The broad peak is associated with <sup>16</sup>O displaced from Na<sub>2</sub>WO<sub>4</sub> by <sup>18</sup>O reacting with H<sub>2</sub>. This broad pulse is not seen on the blank sample indicating that the peak is only generated by the oxygen in Na<sub>2</sub>WO<sub>4</sub>. The broad peak is also not observed when only a broad pulse of H<sub>2</sub> is injected or when a sharp pulse of Ar is used instead of <sup>18</sup>O<sub>2</sub> confirming that the additional water production is due to redox behavior of Na<sub>2</sub>WO<sub>4</sub>.

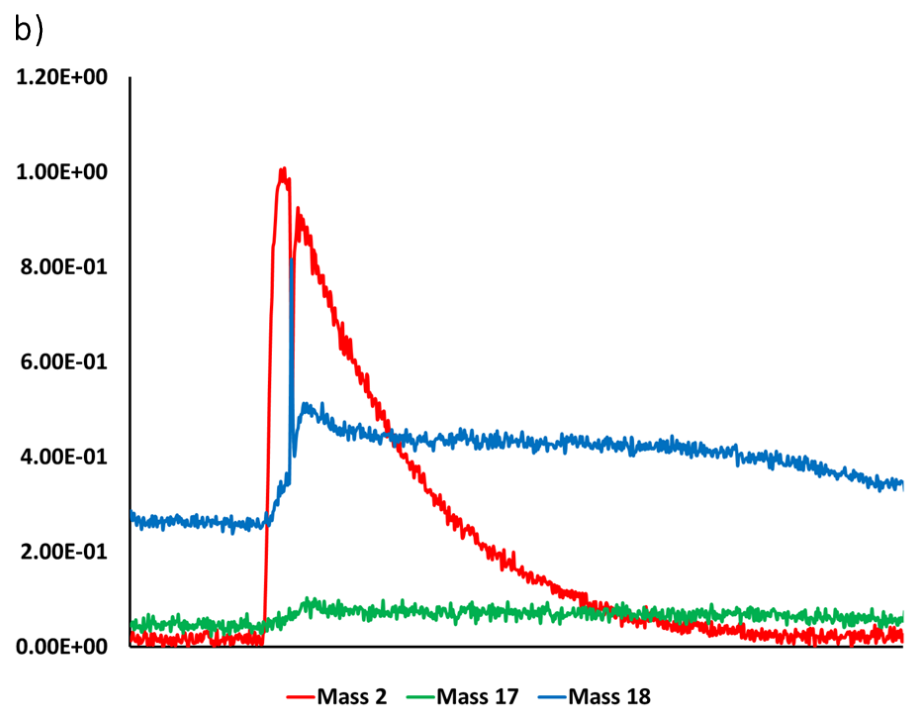
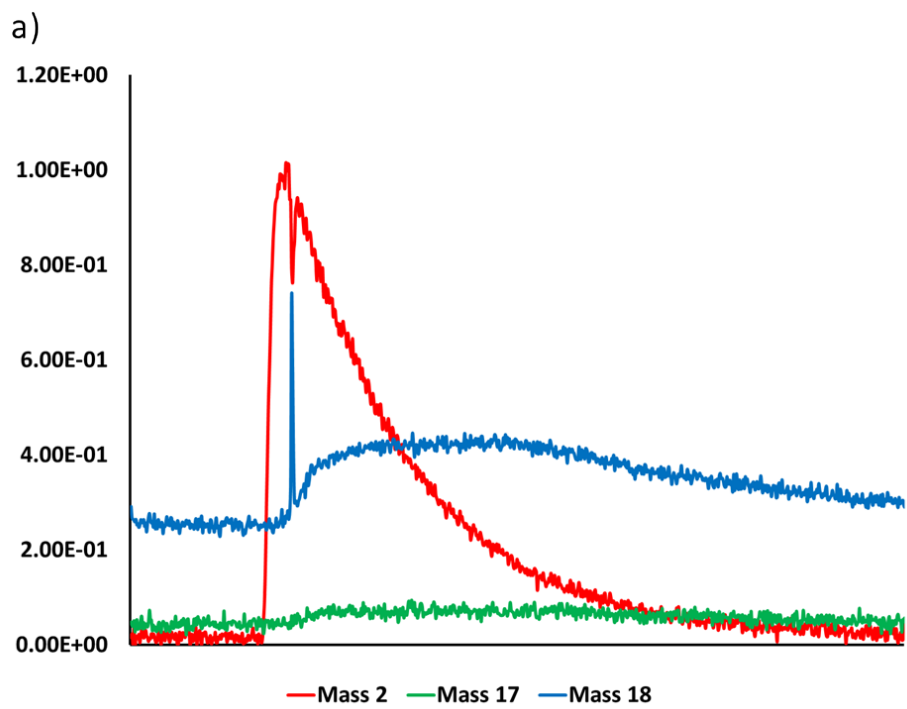


**Figure S5:** Broadened pulse of H<sub>2</sub> with sharp pulse <sup>18</sup>O<sub>2</sub> at 850°C over a) blank and b) 20wt% Na<sub>2</sub>WO<sub>4</sub>/α-Al<sub>2</sub>O<sub>3</sub>

### C<sub>2</sub>H<sub>4</sub>-O<sub>2</sub> co-feed

C<sub>2</sub>H<sub>4</sub>-O<sub>2</sub> co-feed experiments were performed the same way as CO-O<sub>2</sub> and H<sub>2</sub>-O<sub>2</sub> co-feed experiments. Unlike the previous co-feed experiments, we used the production rate of CO<sub>2</sub> to compare the thermal blank and Na<sub>2</sub>WO<sub>4</sub> promoted redox catalyst. This was because gas phase ethylene reactions make direct quantification of ethylene conversion with mass spec difficult.

We did not test the un-promoted redox catalyst because of its high ethane conversion (81.1%) and CO<sub>x</sub> selectivity (75%) during ODH reaction testing at 800 °C. In a co-feed environment, we would expect an even higher CO<sub>2</sub> production due to the presence of gaseous oxygen.

**Table S2:** CO<sub>2</sub> production rate during C<sub>2</sub>H<sub>4</sub>-O<sub>2</sub> co-feed study.

Temperature (°C)	Un-promoted	Na <sub>2</sub> WO <sub>4</sub> promoted
600	5.8*10 <sup>-3</sup> mL/min	1*10 <sup>-2</sup> mL/min
700	2.6*10 <sup>-2</sup> mL/min	2.7*10 <sup>-2</sup> mL/min
800	0.16 mL/min	0.17 mL/min

**Table S3:** Comparison of un-promoted and Na<sub>2</sub>WO<sub>4</sub> promoted redox catalysts

Experiment	Un-promoted	Na:W = 2:1
LEIS	Mg and Mn primary elements on surface of redox catalyst	Na <sub>2</sub> WO <sub>4</sub> forms a shell around the Mg <sub>6</sub> MnO <sub>8</sub> redox catalyst
Methanol TPSR	Basic and redox sites detected	Na <sub>2</sub> WO <sub>4</sub> significantly reduces the amount of basic sites
In-situ DRIFTS	Formate and carbonate species detected. Species still present at 450°C	Only carbonate species detected. No species present at 250°C. Na <sub>2</sub> WO <sub>4</sub> inhibits surface activity for oxidation
CO-O <sub>2</sub> co-feed	Complete conversion of CO at all temperatures	No additional conversion of CO over the thermal blank, Mg <sub>6</sub> MnO <sub>8</sub> is fully covered by Na <sub>2</sub> WO <sub>4</sub>
H <sub>2</sub> -O <sub>2</sub> co-feed	Significantly higher H <sub>2</sub> conversion than thermal blank at all temperature	Solid Na <sub>2</sub> WO <sub>4</sub> : H <sub>2</sub> conversion similar to thermal blank Molten Na <sub>2</sub> WO <sub>4</sub> : H <sub>2</sub> conversion higher than thermal blank, molten Na <sub>2</sub> WO <sub>4</sub> promotes H <sub>2</sub> combustion
<sup>18</sup> O- <sup>16</sup> O exchange	Significant uptake of <sup>18</sup> O and isotopic randomization	Isotopic randomization is suppressed, Na <sub>2</sub> WO <sub>4</sub> shell inhibits O <sub>2</sub> dissociative adsorption
Na <sub>2</sub> WO <sub>4</sub> reduction and gas switching experiments	n/a	Na <sub>2</sub> WO <sub>4</sub> is reducible (albeit slow) and the sample combusts hydrogen by

		shuttling oxygen from Mg <sub>6</sub> MnO <sub>8</sub>
ODH Reaction testing (850°C)	Ethylene Yield:13.29%	Ethylene Yield: 62.17%

## **References**

- (1) Toby, B. H.; Von Dreele, R. B. *GSAS-II: The Genesis of a Modern Open-Source All Purpose Crystallography Software Package*. *J. Appl. Crystallogr.* **2013**, *46* (2), 544–549.  
<https://doi.org/10.1107/S0021889813003531>.